The apoptotic engulfment protein Ced-6 participates in clathrin-mediated yolk uptake in *Drosophila* egg chambers

Anupma Jha, Simon C. Watkins, and Linton M. Traub
Department of Cell Biology and Physiology, University of Pittsburgh School of Medicine, Pittsburgh, PA 15261

ABSTRACT **Clathrin-mediated endocytosis and phagocytosis are both selective surface internalization processes but have little known mechanistic similarity or interdependence. Here we show that the phosphotyrosine-binding (PTB) domain protein Ced-6, a well-established phagocytosis component that operates as a transducer of so-called "eat-me" signals during engulfment of apoptotic cells and microorganisms, is expressed in the female *Drosophila* germline and that Ced-6 expression correlates with ovarian follicle development. Ced-6 exhibits all the known biochemical properties of a clathrin-associated sorting protein, yet *ced-6*–null flies are semifertile despite massive accumulation of soluble yolk precursors in the hemolymph. This is because redundant sorting signals within the cytosolic domain of the *Drosophila* vitellogenin receptor Yolkless, a low density lipoprotein receptor superfamily member, occur; a functional atypical dileucine signal binds to the endocytic AP-2 clathrin adaptor directly. Nonetheless, the Ced-6 PTB domain specifically recognizes the noncanonical Yolkless FXNPXA sorting sequence and in HeLa cells promotes the rapid, clathrin-dependent uptake of a Yolkless chimera lacking the distal dileucine signal. Ced-6 thus operates in vivo as a clathrin adaptor. Because the human Ced-6 orthologue GULP similarly binds to clathrin machinery, localizes to cell surface clathrin-coated structures, and is enriched in placental clathrin-coated vesicles, new possibilities for Ced-6/Gulp operation during phagocytosis must be considered.**

Monitoring Editor
Patrick J. Brennwald
University of North Carolina

Received: Nov 22, 2011
Revised: Feb 28, 2012
Accepted: Mar 2, 2012

INTRODUCTION

In oviparous animals, all the nutritional requirements for embryonic development are met by the deposition of a yolk store during oogenesis. This is necessary until eclosed progeny can feed independently, as early development occurs in the absence of any maternal support. Yolk typically consists of core phosphoglycolipoproteins cached in highly concentrated (often crystalline) form within mature yolk granules or spheres—membrane-bounded intracellular organelles in the oocyte cytoplasm; yolk is the major proteinaceous constituent of unfertilized eggs. In most organisms, yolk protein precursors (vitellogenins) are not synthesized by the oocyte but are instead produced by nongermline cells in a hormonally regulated manner (Raikhel and Dhadialla, 1992). This makes the uptake and storage of yolk dependent on the endocytic apparatus, and, in fact, some of the earliest images of clathrin-mediated endocytosis come from ultrastructural analysis of developing eggs (Anderson, 1964; Roth and Porter, 1964; Perry and Gilbert, 1979). Termed vitellogenesis, the intense accumulation of yolk by the oocyte occurs at a fixed period during oocyte maturation and, since the immediate source of yolk precursors is the extracellular space, is terminated by deposition of the eggshell enshrouding the mature egg by the somatic follicular epithelium. This places temporal restrictions on the massive burst endocytic activity necessary to sequester a yolk depot that is ultimately critical to reproductive success.

This article was published online ahead of print in MBoC in Press (http://www.molbiolcell.org/cgi/doi/10.1091/mbc.E11-11-0939) on March 7, 2012.

A.J. and L.M.T. designed the research plan, conducted experiments, and interpreted the data. S.C.W. produced the ultrastructural data. L.M.T. wrote the manuscript.

The authors declare that they have no conflict of interest.

Address correspondence to: Linton M. Traub (traub@pitt.edu).

Abbreviations used: BSA, bovine serum albumin; CLASP, clathrin-associated sorting protein; ER, endoplasmic reticulum; EST, expressed sequence tag; GFP, green fluorescent protein, GST, glutathione *S*-transferase; His_6, hexahistidine; IgG, immunoglobulin G; LDL, low density lipoprotein; mAb, monoclonal antibody; mcRFP, monomeric Cherry red fluorescent protein; PTB, phosphotyrosine binding; PtdIns(4,5)P_2, phosphatidylinositol 4,5-bisphosphate; RAP, receptor-associated protein; siRNA, small interfering RNA; tdRFP, tandem dimer Tomato red fluorescent protein; VLDL, very low density lipoprotein.

In the disease vector mosquitoes *Anopheles gambiae* and *Aedes aegypti*, a blood meal triggers production of vitellogenin and the lipoprotein-like transporter lipophorin by the fat body and release into the hemolymph. The biosynthesis of the vitellogenin and structurally related lipophorin receptors in developmentally repressed oocytes is also up-regulated by imbibing blood (Cho and Raikhel, 2001; Seo *et al.*, 2003; Atella *et al.*, 2006), which then orchestrate the concentration and transfer of yolk precursors into the egg using clathrin-coated intermediates (Roth and Porter, 1964; Anderson and Spielman, 1971; Snigirevskaya *et al.*, 1997). Blood ingestion thus synchronizes a wave of oocyte maturation, and eggs uniformly enlarge ~300-fold within 48 h. The vitellogenin and lipophorin receptors are members of the low density lipoprotein (LDL) receptor superfamily, which typically use the [FY]XNPX[YF]-type sorting signal for incorporation into clathrin coats. This peptide internalization signal is decoded by a subset of clathrin-associated sorting proteins (CLASPs) characterized by an N-terminal phosphotyrosine-binding (PTB) domain (Traub, 2009). Both *A. aegypti* and *A. gambiae* express trephin, which is transcriptionally regulated by a blood meal (Mishra *et al.*, 2008). This PTB-domain CLASP binds physically to receptors, phosphatidylinositiol 4,5-bisphosphate ($PtdIns(4,5)P_2$), the heterotetrameric AP-2 clathrin adaptor, and clathrin to drive cargo packaging (Mishra *et al.*, 2008).

Unlike mosquitoes, the typical *Drosophila* ovary develops asynchronously, with individual ovarioles each containing a staggered series of progressively more mature egg chambers. Still, clathrin-coated structures are abundant at the oolemma of vitellogenic-stage eggs (Mahowald, 1972; DiMario and Mahowald, 1987; Sommer *et al.*, 2005; Compagnon *et al.*, 2009). Three mutants incontrovertibly demonstrate the involvement of clathrin-dependent endocytosis in *Drosophila* yolk accumulation. First, in the germline, three clathrin heavy chain–null alleles cause a penetrant female sterility (Bazinet *et al.*, 1993). Second, a temperature-sensitive form of the large endocytic GTPase dynamin, expressed in the *shibire* mutant (van der Bliek and Meyerowitz, 1991), disrupts yolk uptake. Within 5 min at the restrictive temperature, the prominent cortical endocytic compartment vanishes, whereas, reciprocally, extracellular yolk precursors, the oocyte surface area, and attached spherical clathrin profiles increase markedly (Kessell *et al.*, 1989; Tsuruhara *et al.*, 1990). On return to the permissive temperature, the arrested clathrin structures bud, swiftly regenerating the lost early endosomal elements (Kessell *et al.*, 1989; Tsuruhara *et al.*, 1990). These experiments also reveal the choreographed sequence of membrane transformations during yolk granule maturation, highlighting this as an archetypical endosomal sorting process.

Third, the vitellogenin receptor orthologue in *Drosophila melanogaster* is designated Yolkless (Schonbaum *et al.*, 1995; Sappington *et al.*, 1996), mutant alleles of which derive from female sterile screens (Bakken, 1973; Tedesco *et al.*, 1981; Waring *et al.*, 1983; DiMario and Mahowald, 1987). Mature eggs from homozygous *yolkless* mutant females shrivel, and strong alleles cause ~10-fold decrease in clathrin-coated profiles at the oolemma of vitellogenic egg chambers (DiMario and Mahowald, 1987). Yolkless is unusual in that the cytosolic FXNPXY-type sorting signal is a nonstandard ^{1837}FQNPLA, albeit positioned at the appropriate distance from the inner leaflet of the bilayer (Schonbaum *et al.*, 1995; Tufail and Takeda, 2009). This FQNPLA sequence is perfectly conserved in 11 other *Drosophila* species (Clark *et al.*, 2007; Supplemental Figure S1). Yet, for the structurally and functionally related LDL receptor in mammals, a Tyr → Ala substitution in the FDNPVY sorting signal decreases internalization >80% (Chen *et al.*, 1990). In addition, Drosophilidae do not express an immediate trephin orthologue, suggesting that Yolkless may have a dedicated cognate CLASP and/or alternative sorting signal(s) to ensure efficient packaging into clathrin-coated structures during vitellogenesis. In this study we report novel data revealing that Ced-6, a PTB-domain adaptor that participates in the phagocytic uptake of bacteria, cell debris, and apoptotic cell corpses in *D. melanogaster* (Awasaki *et al.*, 2006; Cuttell *et al.*, 2008; Fuentes-Medel *et al.*, 2009) and *Caenorhabditis elegans* (Liu and Hengartner, 1998; Smits *et al.*, 1999), is an oocyte CLASP that participates in Yolkless uptake within clathrin-coated vesicles.

RESULTS

The ovary—the biggest organ in the adult *Drosophila* female—is composed of ~15 parallel ovarioles (King, 1970). During oogenesis, egg chambers within an ovariole progress through 14 morphologically discrete stages as they approach the oviduct, resulting in mature eggs ready for fertilization and subsequent embryonic development. Yolk storage is a vital aspect of oocyte maturation and, in *D. melanogaster*, generally occurs over ~16 h between stages 8 and 11. By contrast, the last previtellogenic stage—stage 7—lasts ~9 h (King, 1970). Within an individual ovariole, then, only a subset of egg chambers is actively vitellogenic. This is clearly seen in dissected ovaries incubated either with trypan blue or monomeric Cherry red fluorescent protein (mcRFP)–receptor-associated protein (RAP), an endoplasmic reticulum (ER) chaperone and pseudoligand for LDL receptor superfamily members (Bu, 2001). In both cases, only ovate egg chambers are labeled, with the cortical region of the posteriorly positioned oocyte visibly colored (Figure 1, A–C). The added extracellular endocytic tracers pass between the patent somatic epithelium into the space between the follicle cell apical surface and the oolemma, where they, like yolk precursors proper, are endocytosed rapidly by clathrin-mediated endocytosis (Figure 1D). The 15 anterior germline nurse cells, physically connected to the oocyte, do not accumulate yolk or appreciably take up tracers because the principal yolk precursor receptor, Yolkless, is translated only in the oocyte (Figure 1E; Schonbaum *et al.*, 2000; Coutelis and Ephrussi, 2007). In vitellogenic chambers, the localization of clathrin largely parallels that of the cortically relocated Yolkless (Figure 1, F and G). In fact, the intracellular positioning of clathrin changes with the onset of the immense burst of endocytosis at stage 8, from bright, large, intracellular clusters (Figure 1, F and H) to a diffuse cortical pattern within the oocyte. The clathrin does not relocalize similarly in the anterior nurse cells, consistent with the lack of internalization of lipophorin receptors in these germline cells (Parra-Peralbo and Culi, 2011). Limited cortical clathrin deposition also agrees with clathrin- and AP-2–independent induction of follicle cell Notch signaling by germline Delta in stage 6 signal-sending cells (Windler and Bilder, 2010; Banks *et al.*, 2011).

Ced-6 expression in the fly ovary

LDL receptor superfamily members like Yolkless are generally recognized by PTB-domain CLASPs for internalization (Traub, 2009), and ARH orthologues operate in yolk storage in *Xenopus* (Zhou *et al.*, 2003) and mosquitoes (Mishra *et al.*, 2008). However, phylogenetic dendrograms (TreeFam TF314159; Ruan *et al.*, 2008) reveal that *Drosophila* species do not have an immediate ARH/trephin orthologue and that in *D. melanogaster* the most closely related PTB-domain protein to these endocytic factors is Ced-6 (CG11804; Tamborindeguy *et al.*, 2010). Ced-6 is an orthologue of the *C. elegans* CED-6 protein that participates in the engulfment of apoptotic cell corpses (Liu and Hengartner, 1998; Smits *et al.*, 1999).

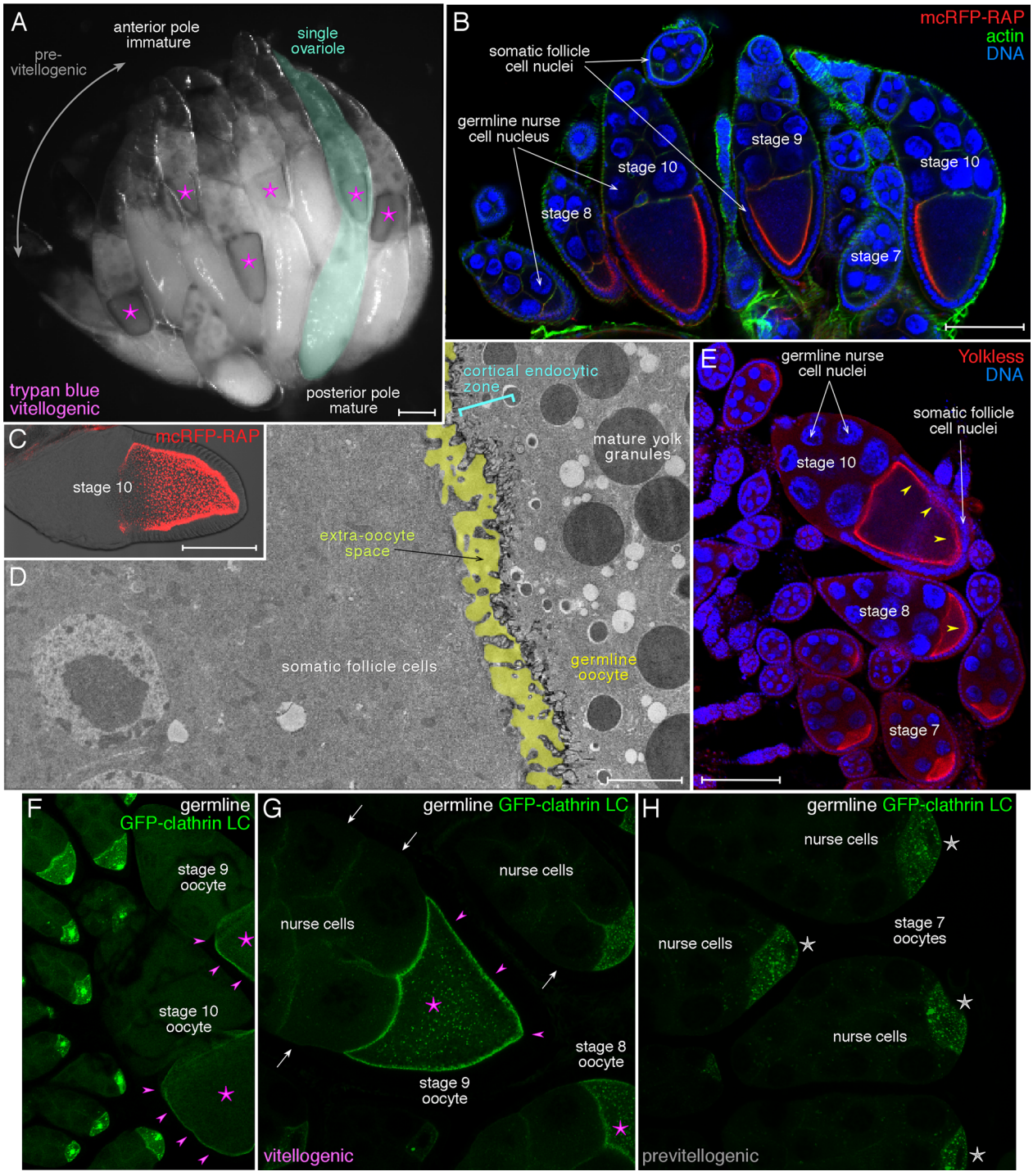

FIGURE 1: Rapid endocytosis in the *Drosophila* ovary. (A) Endocytic uptake by vitellogenic (asterisks) stage Canton-S egg chambers revealed by in vitro incubation with trypan blue for 15 min. (B, C) Selective oocyte internalization of soluble RAP in dissociated vitellogenic egg chambers after incubation with soluble mcRFP-RAP for 20 min. Representative confocal image counterstained with Alexa 488–phalloidin and Hoechst 33342 for DNA (B) or with differential interference contrast (C). (D) Thin-section micrograph of the cortical oocyte–follicle cell region (vitellogenic stage 10) highlighting the active endocytic zone and extra-oocyte space (pseudocolored). (E) Confocal section showing germline expression and oocyte-specific localization (arrowheads) of Yolkless in dissociated Canton-S egg chambers counterstained for DNA. (F–H) Confocal images of localization of clathrin in germline triple-driver Gal4 UAS-GFP-clathrin light-chain (LC) fly egg chambers. Arrowheads indicate cortical deposition in oocytes (asterisk) while little clathrin masses on the cortical plasma membrane of nurse cells (arrows). Scale bar, 100 μm; 2 μm in D.

Unlike the ~300-residue vertebrate CED-6 orthologue (termed Gulp; Liu and Hengartner, 1999; Su *et al.*, 2002) and related ARH proteins, these PTB-domain adaptors are larger (~500 amino acids; Figure 2A), although CED-6/Gulp function is conserved (human GULP can partially complement a *ced-6*–mutant worm; Liu and Hengartner, 1999; Smits *et al.*, 1999).

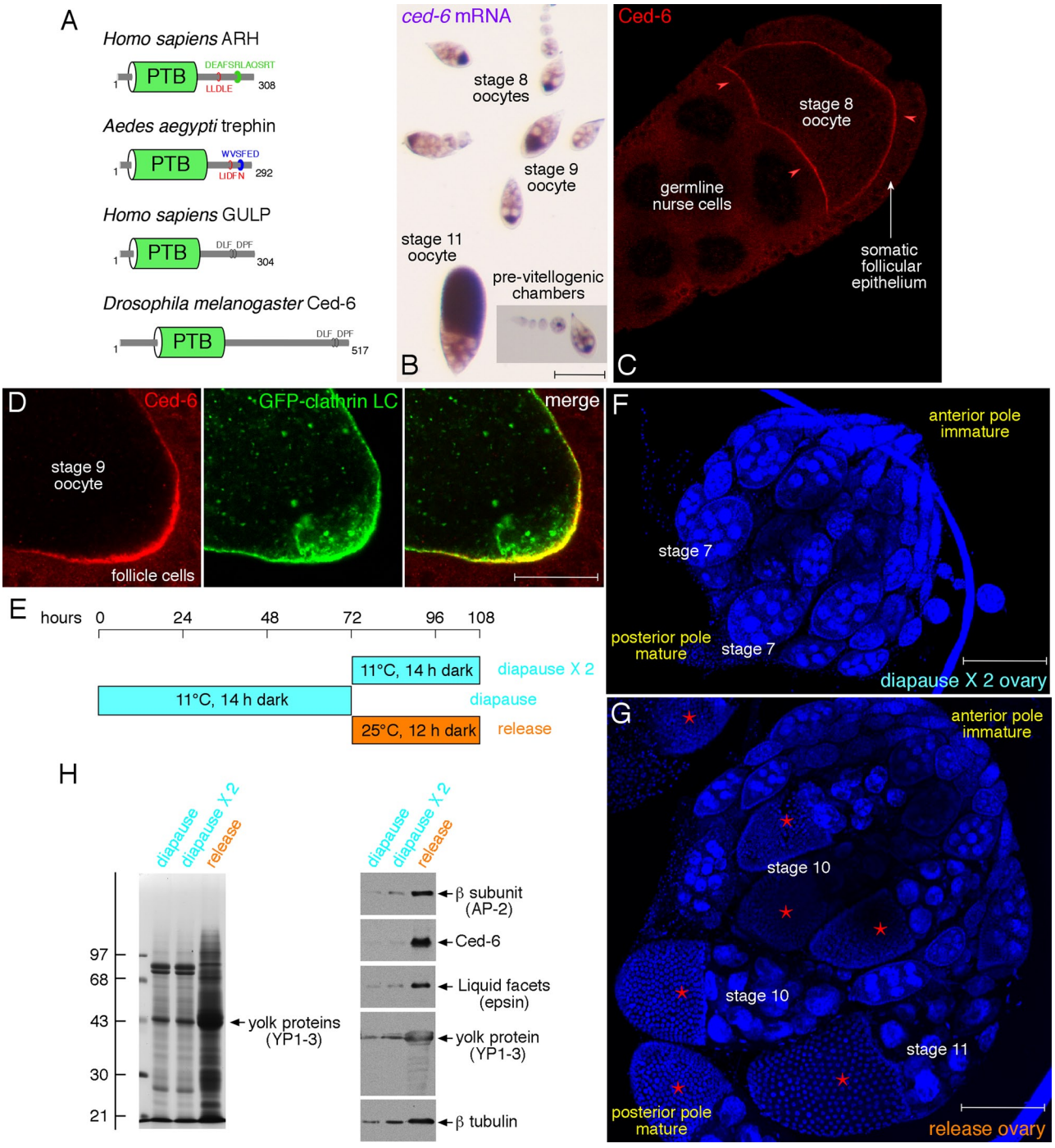

FIGURE 2: Germline Ced-6 expression in fly oocytes. (A) Architectural relationship between various ARH and Ced-6 proteins. The position of clathrin-binding (red) and AP-2–binding (green, blue, gray) sequence motifs is indicated. (B) Whole-mount in situ hybridization analysis of *Ced-6* transcript expression in *D. melanogaster* ovarioles. Dissected ovaries from Canton-S females were analyzed with a DIG-labeled *ced-6* antisense riboprobe. Scale bar, 250 μm. C) Confocal image of the positioning of Ced-6 in the oocyte. (D) Colocalization of germline Ced-6 and clathrin at oocyte cortex. (E) Experimental setup for the induction of diapause and release. (F, G) Morphological difference between dissected diapause (F) and released (G) ovaries stained for DNA. A representative single optical section of each is shown. Note vitellogenic chambers (asterisks) and that diapause ovaries arrest prior to stage 8. Scale bar, 150 μm. (H) SDS–PAGE analysis of four ovary equivalents/lane from dissected diapause or released ovaries stained (left) or immunoblotted (right) with antibodies against the indicated proteins. The positions of the mass standards in kilodaltons are indicated.

Drosophila egg chambers contain mRNA transcripts for Ced-6 within germline-derived oocyte and associated nurse cells, which deposit RNA into the transcriptionally quiescent oocyte (Figure 2B). Like trephin mRNA in *A. aegypti* (Mishra *et al.*, 2008), relative expression of the message is low in previtellogenic chambers but high in the endocytic stages. Accordingly, the Ced-6 protein is concentrated at the oocyte cortex, particularly at the posterior end, where endocytic activity is

highest (Vanzo *et al.*, 2007). Ced-6 expression is restricted to vitellogenic follicles in a pattern similar to that of cortical clathrin (Figure 2D).

In unfavorable environments, female *Drosophila* can enter a period of reproductive diapause (Saunders *et al.*, 1989), a seasonal adaptation coupling reproduction to suitable surroundings. During diapause, ovariole development arrests at a previtellogenic stage in an energy-conserving dormancy. Ovaries from females incubated at 11°C with a 14-h-dark photoperiod contain only prolate spheroid egg chambers, with nurse cells and adjacent oocytes of similar size (Figure 2, E and F). On shift to 25°C a synchronous burst of oocyte maturation ensues. Egg chambers become oblong ovals, the oocyte increases greatly in size, and the follicle cell nuclei reorient over the expanding oocyte (Figure 2G). Release from diapause correlates with a sharp increase in Ced-6 protein levels in the ovary, paralleling other endocytic components and the large accumulation of yolk protein precursors (Figure 2H). This indicates that like trephin in mosquitoes (Mishra *et al.*, 2008), Ced-6 is heavily produced when vitellogenesis begins. These data therefore correlate transcriptional regulation and cortical positioning of Ced-6 with the inception of yolk uptake in the fly ovary.

Endocytic features of the Ced-6 protein

Ced-6 orthologues comprise an N-terminal PTB domain, an adjacent coiled-coil domain promoting dimerization (Su *et al.*, 2000), and an intrinsically unstructured C-terminal segment of variable length (Smits *et al.*, 1999). The PTB plus coiled-coil domain (residues 1–300) of *Drosophila* Ced-6 binds selectively to PtdIns(4,5)P_2-containing synthetic liposomes (Figure 3A), analogous to the PTB domains of ARH and trephin (Mishra *et al.*, 2002b, 2008). The affinity of the N-terminal segment of Ced-6 is at least eightfold higher for phosphoinositide-containing membranes.

All CLASPs bind physically to AP-2 or clathrin, although most engage both core coat components through tandemly arrayed sequences (Reider and Wendland, 2011). Intact *Drosophila* Ced-6 fused to glutathione *S*-transferase (GST) likewise engages both AP-2 and clathrin in pull-down assays, as effectively as ARH (Figure 3B) or trephin (Mishra *et al.*, 2008), despite no obvious extended sequence homology outside of the PTB domains. The clathrin heavy chain and the large (~100 kDa) AP-2 α and β subunits are the principal binding partners on stained gels, but clathrin light chains and the AP-2 μ2 subunit are confirmed on immunoblots. In the silkworm *Bombyx mori* the Ced-6 homologue (NM_001177859, ~39% overall identity with *D. melanogaster*) is implicated in phagocytosis of bacteria in larvae and adults; *ced-6* transcripts are up-regulated within 3 h of bacterial challenge (Ishii *et al.*, 2010). However, an expressed sequence tag (EST) clone for *ced-6* is derived from an ovary library, possibly suggesting a similar role to the *Drosophila* Ced-6. Fused to GST, the full-length *B. mori* Ced-6 also associates with AP-2 and clathrin (Figure 3B). By contrast, the human orthologue, GST-GULP (23% overall identity with *D. melanogaster* Ced-6), binds to AP-2 comparably with *Drosophila* and *B. mori* Ced-6, but clathrin engagement is substantially weaker.

The AP-2– and clathrin-binding determinants are located in the C-terminal portion of Ced-6, as residues 285–517 fused to GST associate with these proteins as avidly as the full length (Figure 3C). AP-2– and clathrin-binding sites within *Drosophila* Ced-6 are bipartite. The entire C-terminal region (residues 285–517) is only weakly affected by mutation of the ^{486}DPF tripeptide to APA, whereas a shorter C-terminal segment (residues 401–517) is strongly affected; the GST-Ced-6 (285–517; DPF → APA) fusion binds to the core coat components similarly to the GST-Ced-6 (401–517; Figure 3D).

Durable clathrin-binding properties

An important interaction element is clearly located at the C-terminus of *Drosophila* Ced-6, as neither residues 401–468 nor 401–500 fused to GST bind to clathrin as efficiently as residues 401–517 or 475–517 (Figure 3C). This C-terminal extension is characteristic of Ced-6 from various insects, like the PTB-domain loop insertion (Supplemental Figure S2). Comparison of this region in insect Ced-6 counterparts reveals two sequence tracts: the proximal D[LP]F region conserved in *Drosophila* and a more evolutionarily conserved distal sequence rich in acidic and leucine side chains, resembling established clathrin box sequences (Supplemental Figure S2). Both portions contribute to clathrin binding, as recovery of clathrin is substantially diminished if either is removed (Figure 3E). The AP-2 association, however, depends on the DPF triplet; inactivation of the ^{486}DPF to APA in the GST-Ced-6 (475–517) backbone disrupts AP-2 binding and reduces clathrin engagement to about the level seen for the C-terminal tract (493–517) alone (Figure 3E). Concordantly, the analogous region of the *B. mori* Ced-6 (residues 471–513) binds to clathrin with a similar apparent affinity as the *D. melanogaster* (493–517) protein, and this silkworm Ced-6 segment does not contain proximal D[LP]F motifs and does not engage AP-2 efficiently. Clearly the primary AP-2–binding information in the *B. mori* Ced-6 (Figure 3B) is not positioned at the C-terminus. Together, these biochemical data indicate that there are multiple clathrin and AP-2 interaction determinants within the C-terminal half of Ced-6.

Binding to AP-2 involves the appendage domains of both the large α and β2 subunits (Figure 3F), analogous to the authentic endocytic proteins eps15, epsin 1, AP180, and intersectin 1 (Lundmark and Carlsson, 2002; Edeling *et al.*, 2006; Schmid *et al.*, 2006; Pechstein *et al.*, 2010). The overlap reflects both the structural homology between the AP-2 α and β2 appendages and the fact that interaction motifs for the four different contact sites on the appendages all use exposed aromatic side-chain anchor residues (e.g., DP[FW], FXDXF, and WXX[FW] motifs), and there is substantial binding promiscuity (Schmid and McMahon, 2007; Traub, 2009). Binary interaction assays confirm that the association with Ced-6 is direct and reveal that, for the β2 appendage, binding occurs via the platform subdomain, as it is disrupted by a Y888M substitution (Supplemental Figure S3). Overall, these salient biochemical properties are consistent with Ced-6 operating as a CLASP, and ectopic expression of *Drosophila* Ced-6 in HeLa cells reveals an extensive degree of overlap with endogenous AP-2 at scattered puncta on the ventral cell surface (Figure 4A). AP-2, eps15, and expressed Ced-6–green fluorescent protein (GFP) all cocluster at discrete patches on the cell surface (Figure 4B); Ced-6 is thus directed to clathrin-coated structures at steady state. In addition, Ced-6 is a phosphoprotein (Bodenmiller *et al.*, 2007; Zhai *et al.*, 2008), and exposing Ced-6-GFP–expressing HeLa cells to the broad-specificity phosphatase inhibitor calyculin A (Ishihara *et al.*, 1989) significantly changes the electrophoretic mobility of the fusion protein (Figure 4C). This resembles the gel shift of numerous CLASPs and endocytic accessory factors that accompanies calyculin A administration (Lauritsen *et al.*, 2000). Ced-6 can thus undergo dynamic cycles of phosphorylation–dephosphorylation (Bodenmiller *et al.*, 2007; Zhai *et al.*, 2008) like the endocytic dephosphins (Slepnev *et al.*, 1998). Taken together, our data suggest that Ced-6 is endowed with the common functional properties to interface directly with the nascent endocytic clathrin coat.

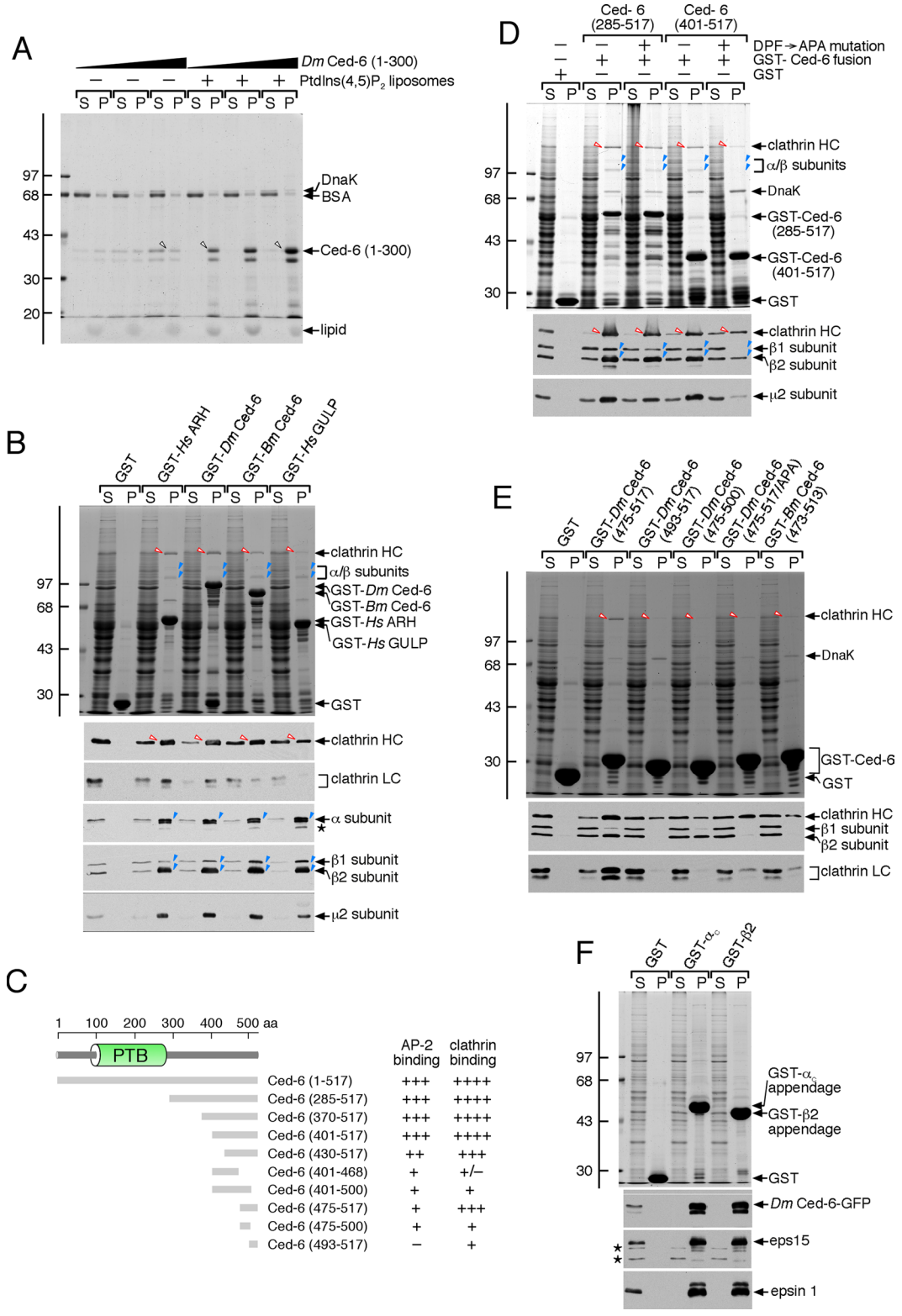

FIGURE 3: Ced-6 is a CLASP. (A) Ced-6 (1–300) (25, 50, or 100 μg/ml), incubated with PtdIns(4,5)P_2-positive or -negative liposomes, was sedimented, and aliquots of each supernatant (S) and pellet (P) were analyzed by SDS–PAGE. Ced-6 (1–300; arrowheads) and the location of the bacterial-derived chaperone DnaK are indicated. (B) Aliquots of S and P fractions from GST pull-down assays with the indicated fusion proteins and brain cytosol were analyzed by SDS–PAGE with staining or immunoblot using the indicated antibodies. The clathrin heavy-chain (HC; red) and AP-2 large subunits (blue) are shown (arrowheads). (C) Semiquantitative tabulation of AP-2 and clathrin binding by the indicated Ced-6 segments fused to GST. (D–F) Aliquots of S and P fractions from GST pull-down assays with the indicated GST fusion proteins and brain cytosol (D, E) or Ced-6-GFP–transfected HeLa lysate (F) were analyzed by SDS–PAGE with staining or immunoblot using the indicated antibodies; Ced-6-GFP was visualized with anti-GFP. The positions of the mass standards in kilodaltons are indicated. LC, light chain.

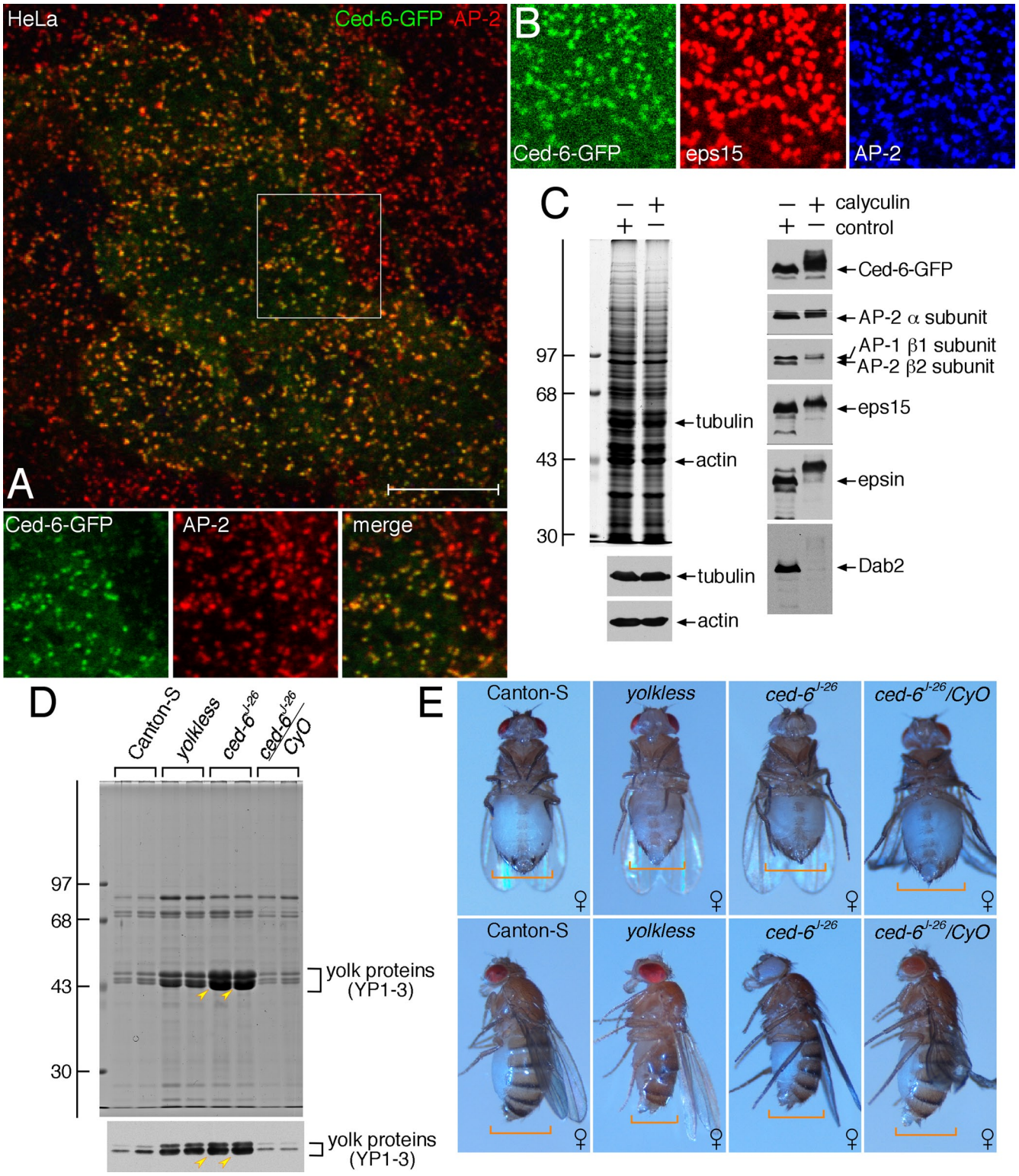

FIGURE 4: Ced-6 is an endocytic protein involved in yolk precursor trafficking. (A) Subcellular localization of transiently expressed Ced-6–GFP in fixed HeLa cells stained with an anti–AP-2 α subunit mAb (red). A representative single confocal optical section is shown, with magnification of the boxed region below. Scale bar, 10 μm. (B) Colocalization of transfected Ced-6–GFP with endogenous eps15 and AP-2 in fixed HeLa cells. A representative, zoomed-in region is shown. (C) Equal aliquots from lysates of Ced-6-GFP–expressing HeLa cells incubated with or without 100 nM calyculin A for 60 min at 37°C were resolved by SDS–PAGE and either stained or immunoblotted with the indicated antibodies. (D) Aliquots of hemolymph (1.5 adult equivalents/lane) from Canton-S, *yolkless*, *ced-6*^{J26}, or *ced-6*^{J26}/CyO females resolved by SDS–PAGE and stained or immunoblotted with anti–yolk protein antiserum. The positions of the three ~43-kDa proteins (YP1-3, arrowheads) and the mass standards in kilodaltons are indicated. (E) Comparison of mature, yeast-fed Canton-S (wild type) with homozygous *yolkless*, *ced-6*^{J26}, or *ced-6*^{J26}/CyO females.

Consistent with these biochemical characteristics, homozygous null *ced-6*^{J26} females (Hashimoto *et al.*, 2009; Kuraishi *et al.*, 2009) massively accumulate circulating yolk proteins (termed YP1-3) in the hemolymph, like female sterile mutants (DiMario and Mahowald, 1987; Gutzeit and Arendt, 1994; Figure 4D). This rules out that the appearance and localization of Ced-6 in the egg chamber are coincidental and not linked directly to yolk uptake. Interestingly, the higher concentration of YP1-3 precursors in the hemolymph of *ced-6*–null females compared with the *yolkless* females could possibly suggest that Ced-6 may also operate in the fat body in a homeostatic yolk recapture process, and, indeed, the FlyAtlas Expression Database (Chintapalli *et al.*, 2007) information for Ced-6 (FBgn0029092) shows very high transcript levels in the adult fat body.

Even so, yeast-fed *ced-6*^{J26} females do have moderately enlarged abdomens, unlike the *yolkless*-null females (Figure 4E), and ultrastructural analysis of ovary sections attests that general vitellogenic egg chamber architecture is preserved. At around stage 10, nurse and follicle cell arrangement is equivalent in *ced-6*^{J26} heterozygous and homozygous chambers (Figure 5, A–H) because major morphogenesis during these stages is largely governed by the surrounding somatic epithelium (Bilder and Haigo, 2012). However, there is a clearly discernible difference in the size of dark, spherical yolk granules within the posteriorly positioned oocyte (Figure 5, A and B). Later, between stages 10B and 11, when the follicle cell–derived vitelline bodies coalesce nearly completely around the oocyte margin, the conspicuous decline in the diameter of *ced-6*^{J26} mature yolk spheres remains (Figure 5, C and D); in *ced-6*^{J26}/CyO oocytes, the yolk granules become progressively larger (Figure 5, A and C). Within the cortical endocytic zone, morphologically discernible clathrin-coated profiles are present in the oolemma of vitellogenic *ced-6*^{J26} oocytes (Figure 5, G and H), but they are decreased in abundance compared with similar-stage *ced-6*^{J26}/CyO egg chambers (Figure 5, E and F). In the vitellogenic stages analyzed, the average yolk granule area decreases from 3.22 to 1.51 μm^2 in *ced-6*^{J26} oocytes, and, correspondingly, the fraction of oocyte cytoplasm containing yolk diminishes from 30 to 14%. These ultrastructural findings link directly the yolk granule abnormalities in the *ced-6*–null ovary to clathrin-coated structures and are a remarkably close phenocopy of weak *yolkless* alleles (DiMario and Mahowald, 1987). By contrast, relative to the heterozygous *ced-6*^{J26}/CyO, the *ced-6*^{J26} egg chambers exhibit a similar distribution of the electron-lucent lipid droplets within germline cells (Figure 5, A and B) confirming the nonendocytic uptake mode through lipophorin receptors in the nurse cells (Parra-Peralbo and Culi, 2011).

Freshly oviposited eggs from homozygous *ced-6*^{J26} females are typically smaller and misshapen, often abnormally translucent, and sometimes collapsed compared with those of heterozygotes (Figure 5, I and J). Nonetheless, *ced-6*–null females are still fertile, although, relative to the heterozygous *ced-6*^{J26}/CyO females, homozygous *ced-6*^{J26} females have substantially reduced fecundity (Figure 5K). This is in general accord with the ultrastructural anomalies seen in vitellogenic egg chambers lacking Ced-6. In *C. elegans*, DAB-1 is similarly involved in yolk accumulation, although *dab-1* mutants are fertile and actually have near-normal brood sizes (Holmes *et al.*, 2007). At least two nonexclusive possibilities could explain the (sub)fertility of the fly *ced-6* mutants. First, Yolkless could deploy several different sorting signals in the cytosolic domain, making recognition by a PTB-domain CLASP unessential. Second, another functionally overlapping PTB-domain CLASP may operate in parallel in the oocyte, as vertebrate ARH and Dab2 do in cultured cells (Keyel *et al.*, 2006; Maurer and Cooper, 2006; Eden *et al.*, 2007; Ezratty *et al.*, 2009).

Endocytic sorting signals in Yolkless

Yolkless is a large (~215 kDa), extensively glycosylated protein (Schonbaum *et al.*, 1995) that requires dedicated ER chaperones (Culi and Mann, 2003), and so, to delineate the endocytic sorting information using HeLa cells, we fused the cytosolic domain of the receptor isoform A to the extracellular and transmembrane segments of Tac, the α chain of the interleukin-2 receptor (CD25; Uchiyama *et al.*, 1981; Figure 6A). Alone, Tac is internalized very slowly in these cells and so serves as a reporter for signal-dependent uptake (Humphrey *et al.*, 1993; Marks *et al.*, 1996; Hawryluk *et al.*, 2006; Pedersen *et al.*, 2010). After incubation with an anti-Tac monoclonal antibody (mAb) on ice, both Tac and Tac-Yolkless are dispersed over the surface of transiently transfected HeLa cells (Figure 6, B and C). Warming the cells to 37°C results in internalization of the surface-labeled Tac-Yolkless and appearance in intracellular endosomes also containing synchronously internalized transferrin (Figure 6, E and F). In these transient transfection experiments, not all the Tac-Yolkless chimera is cleared off the surface of every cell, because high relative expression of the chimera saturates the endocytic machinery (Warren *et al.*, 1998). Tac remains essentially at the surface and in filopodial extensions at 37°C, although transferrin internalizes promptly in these cells into the endosomal compartment (Figure 6D). In uptake assays where transfected cells labeled on ice with an Alexa 546–conjugated anti-Tac mAb are warmed to 37°C before fixation and reprobing nonpermeabilized cells with an Alexa 633–conjugated anti–mouse immunoglobulin G (IgG), the dispersed overlapping (magenta) Tac signal confirms the surface localization. Maximal projections of serial confocal *z*-sections show diffuse staining after 5 or 10 min at 37°C (Figure 6, G and H). By contrast, in cells expressing Tac-Yolkless, within 5 min the Alexa 546 signal separates from the surface Alexa 633 signal and is now in small peripheral early endosomes, which become larger and brighter at 10 min (Figure 6, I and J). Only cells expressing very high levels of Tac-Yolkless have strong magenta-colored surface labeling. In addition, compared with Tac-Yolkless, Tac is more sensitive to trypsinization, confirming greater abundance at the cell surface (Figure 6K). Yolkless endocytic signals can thus be decoded in HeLa cells, and we used this system for further analysis because the Tac reporter alone is efficiently internalized when transfected into *Drosophila*-derived S2 cells.

In addition to the ^{1837}FXNPXA sequence, the 114-residue Yolkless cytosolic domain contains distally two potential dileucine-like signals, ^{1901}LL and ^{1918}LL (Figure 7A). Truncation shows that the C-terminal tract containing these two speculative signals does direct internalization; removal of the C-terminal 53 residues (S1885X) significantly decreases mAb uptake (Figure 7, B and C), and the fusion protein becomes increasingly susceptible to digestion by extracellular trypsin (Figure 6K). In addition, surface biotinylation-based uptake assays show that both the rate and extent of either Tac or Tac-Yolkless (S1885X) internalization are considerably diminished compared with Tac-Yolkless (Figure 7E). The ^{1837}FXNPXA signal alone is thus poor at directing uptake in HeLa cells.

Further analysis indicates that the membrane-proximal ^{1909}LL sequence does not drive efficient internalization, whereas the distal ^{1918}LL sequence can; a L1918A/L1919A (LL1919AA) mutant stalls at the cell surface (Figure 7D). Two lines of evidence together indicate that the Yolkless ^{1918}LL signal is recognized physically by AP-2. First, small interfering RNA (siRNA) silencing of the AP-2 α-subunit mRNA leads to accumulation of both transferrin (Hinrichsen *et al.*, 2003; Motley *et al.*, 2003; Huang *et al.*, 2004) and Tac-Yolkless at the cell surface, whereas adjacent nonsilenced cells internalize both reporters effectively (Figure 7, F–I, and Supplemental Figure S4).

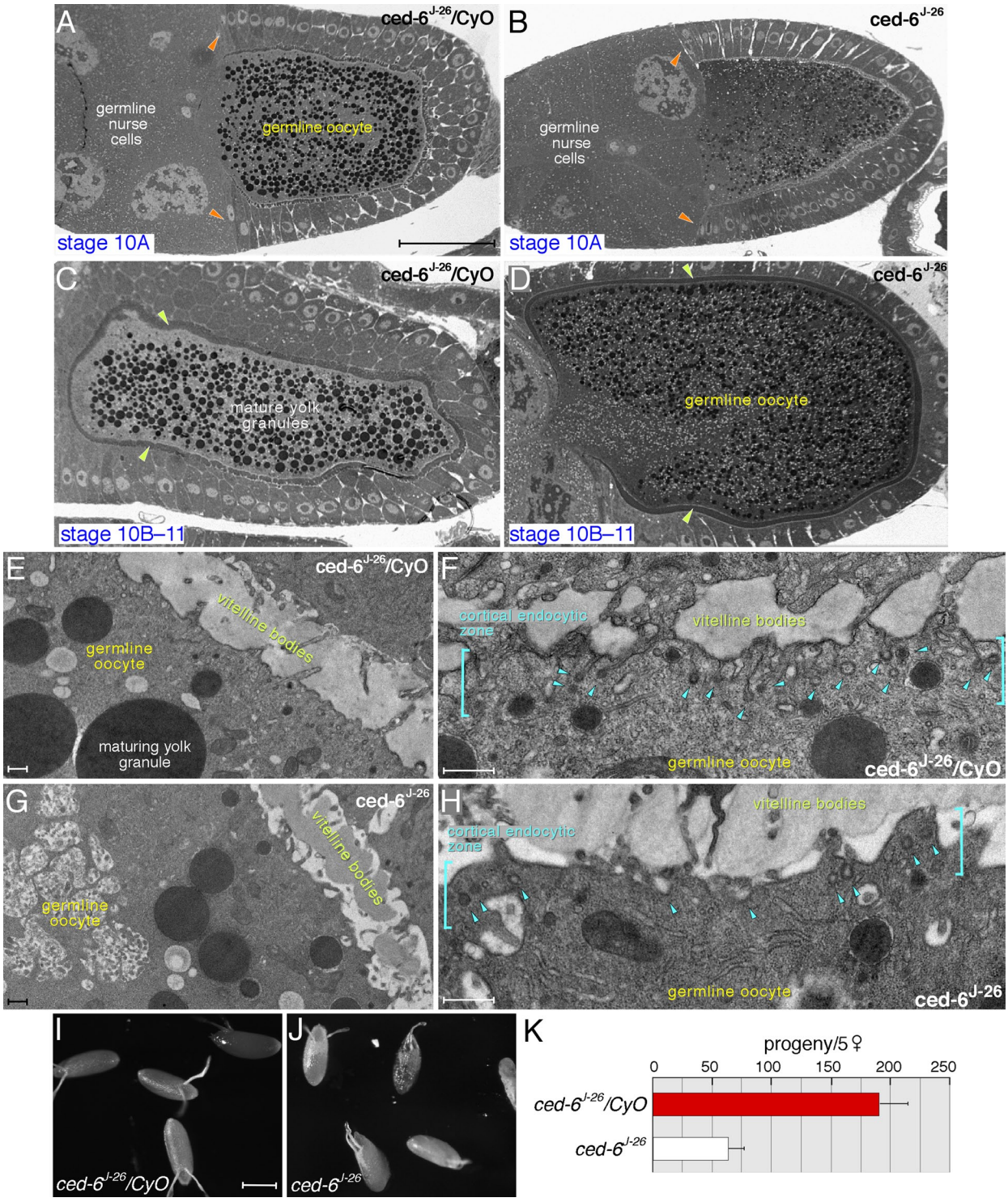

FIGURE 5: *ced-6*^{J26}-null egg chambers are morphologically and reproductively defective. (A–D) Representative bright-field images of toluidine blue–stained, semithin sections of *ced-6*^{J26}*/CyO* and *ced-6*^{J26} egg chambers. Around stage 10A (A, B), identified by relocation (and columnar morphology) of somatic follicle cells to the anterior margin of the oocyte (arrowheads), *ced-6*^{J26}*/CyO* and *ced-6*^{J26} egg chambers are actively vitellogenic. Note, however, the conspicuously decreased number and size of the dark, spherical yolk granules in the *ced-6*^{J26} genetic background. At later vitellogenic stages (10B to 11; C, D), classified by near-complete coalescence of the follicle cell–secreted vitelline bodies around the yolk-laden oocyte (arrowheads), diminutive yolk granules are still present in *ced-6*^{J26} oocytes relative to the heterozygous chambers. Posterior end is to the right. Scale bar, 50 µm. (E–H) Comparative low- and higher-magnification transmission electron micrographs of the cortical region of *ced-6*^{J26}*/CyO* (E, F) or *ced-6*^{J26} (G, H) egg chambers. Scale bar, 500 nm. (I, J) Representative images of freshly oviposited eggs from yeast-fed *ced-6*^{J26}*/CyO* or *ced-6*^{J26} females. Scale bar, 250 µm. (K) Quantitation (mean ± SD) of viable progeny in replicate vials each containing five *ced-6*^{J26} or *ced-6*^{J26}*/CyO* females and three Canton-S males after 2 wk of incubation at 26.5°C. Homozygous *ced-6*^{J26} females are clearly subfertile.

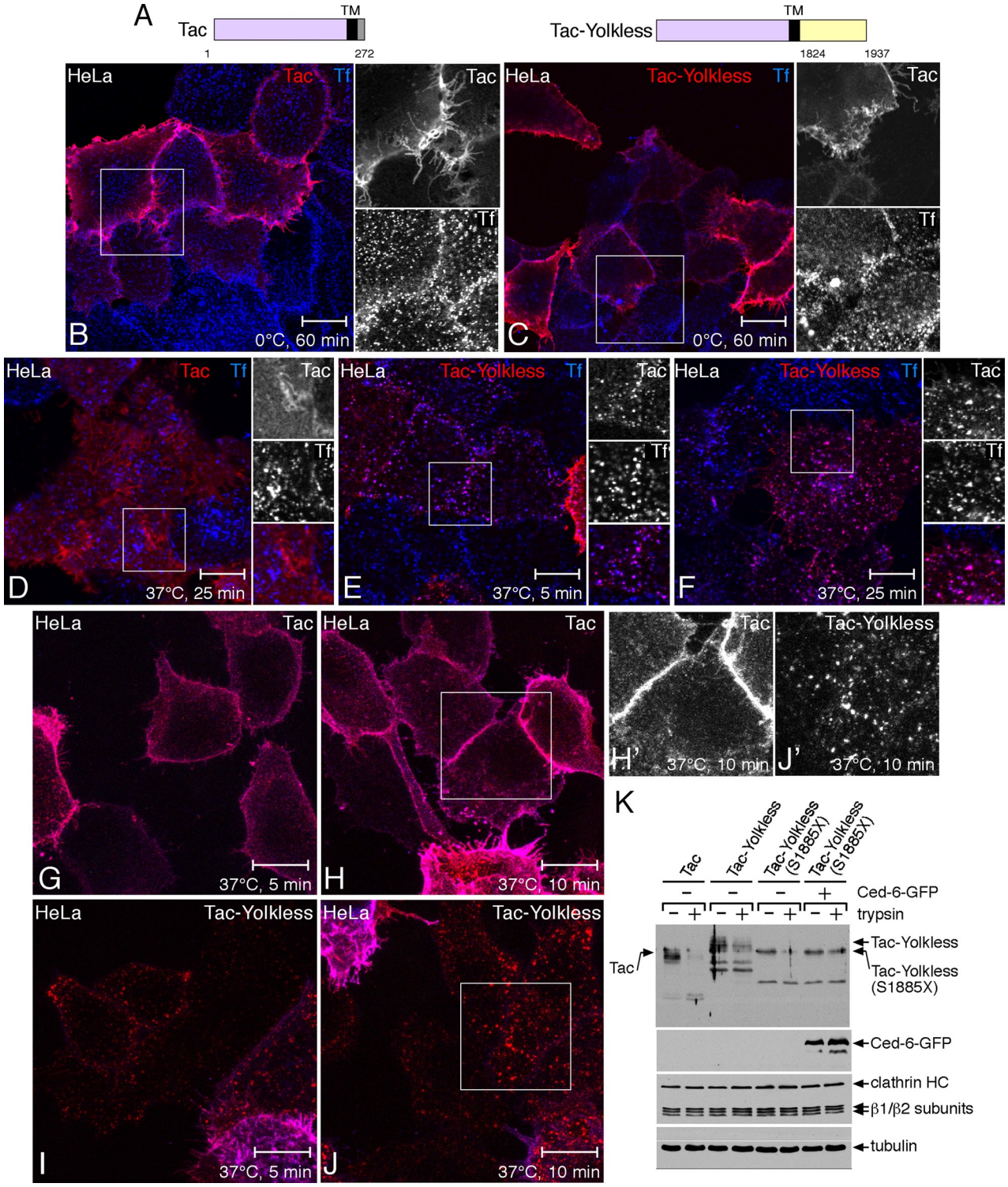

FIGURE 6: Endocytosis of a Tac-Yolkless chimera in mammalian cells. (A) Schematic of constructs. (B–F) Tac (B, D) or Tac-Yolkless (C, E, F) transfected HeLa cells were preincubated with a mixture of anti-Tac mAb and Alexa 633 transferrin (Tf, blue) on ice. Washed cells were either fixed (B, C) or warmed to 37°C for 5 (E) or 25 (D, F) min. Bound anti-Tac was visualized in fixed cells with an Alexa 568 anti-mouse antibody (red). Representative confocal sections are shown, with magnification of the boxed regions shown on the right. (G–J) Tac (G, H) or Tac-Yolkless (I, J) transfected cells were preincubated with Alexa 546–conjugated anti-Tac on ice, washed, and warmed to 37°C for 5 or 10 min. Fixed cells were incubated with an Alexa 633–conjugated anti-mouse antibody without permeabilization. Confocal image stacks projected into a single maximal intensity image are shown with magnification of the red channel from boxed regions shown on the right (H′ and J′). Scale bar, 10 μm. (K) Tac or various Tac-Yolkless fusion protein–expressing HeLa cells cotransfected with Ced-6-GFP as indicated were detached with EDTA (–) or trypsin (+), washed, and solubilized in boiling SDS. Equivalent aliquots were resolved by SDS–PAGE and replicate immunoblots probed with the indicated antibodies; Ced-6–GFP was visualized with anti-GFP.

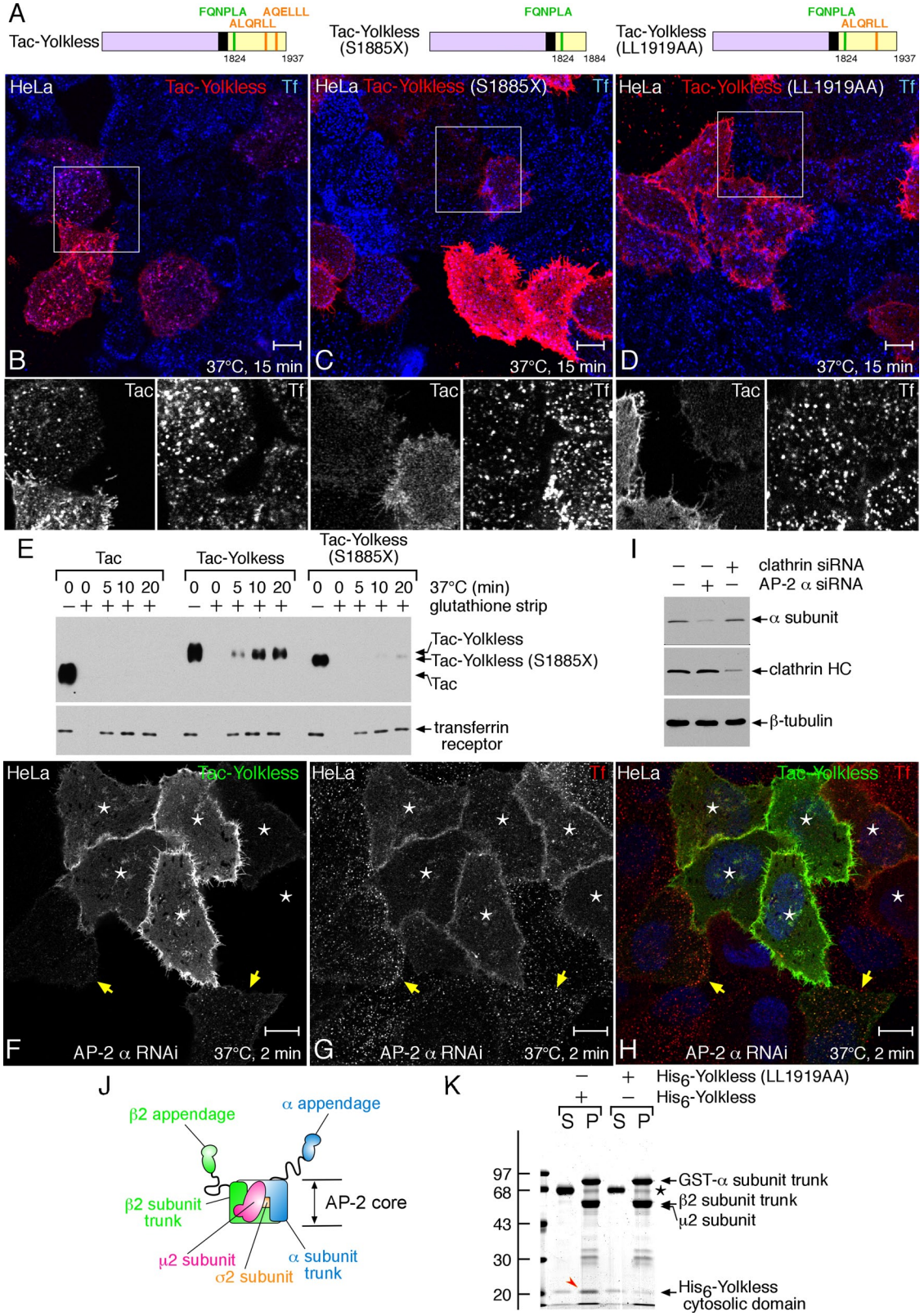

FIGURE 7: An AP-2–dependent dileucine signal in the Yolkless cytosolic domain. (A) Schematic of constructs. (B–D) HeLa cells transfected with Tac-Yolkless (B), Tac-Yolkless (S1885X; C), or Tac-Yolkless (LL1919AA; D) were preincubated with a mixture of anti-Tac mAb and Alexa 633 transferrin (blue) on ice. Washed cells were warmed to 37°C for 15 min and fixed, and bound anti-Tac was visualized with an Alexa 568 anti-mouse antibody (red). Representative confocal optical sections are shown, with magnification of the boxed regions presented below. Scale bar, 10 μm. (E) HeLa cell monolayers transfected with Tac, Tac-Yolkless, or Tac-Yolkless (S1885X) as indicated were surface biotinylated on ice, quenched, and then either held on ice or incubated at 37°C for the indicated times. After stripping of surface-exposed biotin with reduced glutathione on ice, internalized biotinylated proteins in Triton X-100 lysates were recovered with NeutrAvidin

Analogous results are obtained with silencing of the clathrin heavy-chain transcript (Supplemental Figure S4). Second, the heteromeric AP-2 adaptor core, composed of the N-terminal trunks of the large α and β2 chains and the μ2 and dileucine-binding σ2 subunits (Kelly *et al.*, 2008; Jackson *et al.*, 2010; Figure 7J), interacts physically with the Yolkless cytosolic domain in pull-down assays (Figure 7K). The double LL1919AA substitution, which diminishes Tac-Yolkless uptake, decreases the interaction with the purified AP-2 core. These experiments used the mammalian AP-2 core, but the fly σ2 subunit is 93% identical to the murine σ2, and each of the 11 vital residues that form the dileucine contact surface on σ2 (Kelly *et al.*, 2008) is invariant. In addition, the two important basic side chains in the α subunit are unchanged in the 69% identical fly α subunit, as are the two vicinal β subunit aromatics that occlude the dileucine interaction interface in the closed state (Kelly *et al.*, 2008). Collectively these data indicate that Yolkless can interact directly with AP-2 and may explain, in part, the 10-fold decrease in cortical clathrin-coated structures in vitellogenic *yolkless*-mutant oocytes (Schonbaum *et al.*, 2000; Sommer *et al.*, 2005). Surprisingly. however, it has just been reported that AP-2 α or σ2 subunit–null germline clones still efficiently accumulate yolk proteins (Parra-Peralbo and Culi, 2011).

A role for Ced-6 in Yolkless uptake

Although the Yolkless cytosolic domain promotes clathrin-dependent internalization in HeLa cells (Figure 6), the distribution of the Tac reporter on ice changes prominently in cells expressing both Tac-Yolkless and Ced-6-GFP (Figure 8A). Like the Ced-6-GFP, Yolkless now localizes to discrete puncta on the cell surface that are positive for AP-2. Similar clustering of Tac-Yolkless also occurs with truncation at residue 1885 (S1885X), removing the dileucine signal (Figure 8C). Warming the cells to 37°C promotes loss of coincidence with surface Ced-6–GFP and allows prompt internalization of Tac-Yolkless or Tac-Yolkless (S1885X) along with transferrin in the presence of Ced-6 (Figure 8, B and D), but the chimera remains largely at the plasma membrane in cells not also expressing Ced-6 (Figure 8, E and F). Maximal projections of image stacks from Tac-Yolkless (S1885X)–expressing cells reveal that Ced-6 promotes efficient endocytosis within 5–10 min of warming (Figure 8, G and H). Significantly, coexpressing ARH does not permit similar surface clustering or efficient uptake of Tac-Yolkless (S1885X), although ARH-GFP is properly positioned at clathrin-containing puncta (Supplemental Figure S5). However, altering the endogenous Yolkless FXNPXA sequence to a standard FXNPXY signal with an A1842Y substitution leads to analogous clustering and internalization of the Tac-Yolkless (LL1919AA) mutant in the absence of coexpressed Ced-6 (Figure 8, I and J). This confirms there are normally positioned endogenous PTB-domain CLASPs (including ARH and Dab2) that decode FXNPXY signals in clathrin-coated buds, but that the variant sequence in Yolkless is not effectively recognized by these CLASPs. Instead, the PTB domain of *Drosophila* Ced-6 seems uniquely tailored to bind the Yolkless FXNPXA signal. Support for this conclusion comes from the diminished clustering and decreased uptake of Tac-Yolkless (S1885X) in the presence of a cotransfected Ced-6–GFP (S164T/F233V) double mutant (Figure 8, L and M). These two substitutions alter the surface chemistry of the cargo-binding site on the PTB domain (Stolt *et al.*, 2004; Mishra *et al.*, 2008) but do not affect deposition at AP-2–positive clathrin structures (Supplemental Figure S5), indicating that Ced-6 engages the Yolkless FQNPLA sequence through the same molecular surface used by other PTB domains to contact the FXNPXY signal. Both the Tac-Yolkless (S1885X) and (LL1919AA) proteins are efficiently internalized in cells coexpressing Ced-6-GFP, whereas these chimeras remain at the cell surface in the absence of Ced-6 (Figure 8K and Supplemental Figure S6).

We conclude that Ced-6 binds physically to the FQNPLA signal within the Yolkless cytosolic domain but can also recognize regular FXNPXY signals, as Draper, the *Drosophila* homologue of the *C. elegans* engulfment receptor CED-1 (Freeman *et al.*, 2003; Zhou and Yu, 2008), contains a canonical ^{853}FDNPVY sequence that interacts with Ced-6 (Manaka *et al.*, 2004; Awasaki *et al.*, 2006; Hashimoto *et al.*, 2009). Plasticity in recognition of peptide signals is indeed a hallmark of the PTB domain (Farooq and Zhou, 2004; Li *et al.*, 2008) and, in the fly Ced-6, may be related to the insertion within the PTB domain between strands β6 and β7 (Supplemental Figure S2; Kaneko *et al.*, 2011).

Clathrin- and AP-2–binding motifs in Ced-6/GULP

Given that Ced-6/Gulp is an established phagocytic component (Liu and Hengartner, 1998, 1999; Su *et al.*, 2002; Yu *et al.*, 2006, 2008; Zhou and Yu, 2008; Park *et al.*, 2008, 2010), the involvement in Yolkless recognition and uptake raises the possibility of a clathrin-dependent stage(s) in normal phagocytic engulfment. In fact, mammalian GULP binds to clathrin (Martins-Silva *et al.*, 2006; Figure 3B), and, similar to Ced-6-GFP, ectopic GULP-GFP (Kiss *et al.*, 2006) localizes to AP-2–positive structures in HeLa cells (Figure 9A). Given published evidence (Kiss *et al.*, 2006; Martins-Silva *et al.*, 2006; Beyer *et al.*, 2012), it was unexpected that transiently transfected GULP similarly clusters at AP-2–positive surface patches in addition to a diffuse cytosolic pool. Yet the punctate distribution resembles the "granular" staining of endogenous GULP in U-2 OS and U-215 MG cells in the Human Protein Atlas (Uhlen *et al.*, 2010). Analogous results are obtained in HT-1080 cells (Figure 9B), as well as with a tandem dimer Tomato red fluorescent protein (tdRFP)–GULP fusion in HeLa cells (Supplemental Figure S7), albeit with more GULP spots that are not coincident with AP-2. Simultaneous expression of Ced-6-GFP and tdRFP-GULP discloses that both proteins target to the same endocytic clathrin coats (Figure 9C). Similar results are obtained with GULP-GFP and tdRFP-GULP coexpression (Supplemental Figure S7); the general deposition of GULP at clathrin-coated structures is therefore not affected by the positioning of the fused

agarose and detected by immunoblotting after SDS–PAGE. Note that in contrast to whole-cell lysates (Figure 5K), the anti-Tac antibodies only detect the Golgi-processed forms after surface biotinylation, as expected. (F–H) HeLa cells subjected to AP-2 α subunit siRNA were transiently transfected with Tac-Yolkless and then preincubated with a mixture of anti-Tac mAb and Alexa 568 transferrin (red) on ice. Washed cells were warmed to 37°C for 2 min, and then anti-Tac was visualized in fixed cells with an Alexa 488 anti-mouse antibody (green). RNAi-silenced cells (asterisks) accumulate both transferrin and Tac-Yolkless on the surface, whereas adjacent non-silenced cells (arrows) internalize both markers into puncta. (I) Immunoblot analysis of HeLa cell lysates after the indicated siRNA treatments probed with anti–AP-2, clathrin, or tubulin mAbs. (J) Schematic of the AP-2 adaptor complex. (K) Aliquots of S and P fractions from GST pull-down assays with the heterotetrameric GST-tagged AP-2 core and recombinant wild-type (arrowhead) or dileucine mutated (LL1919AA) His_6-Yolkless cytosolic domain were analyzed by SDS–PAGE, resolved by SDS–PAGE, and Coomassie stained. The positions of the mass standards in kilodaltons and carrier BSA (asterisk) are indicated.

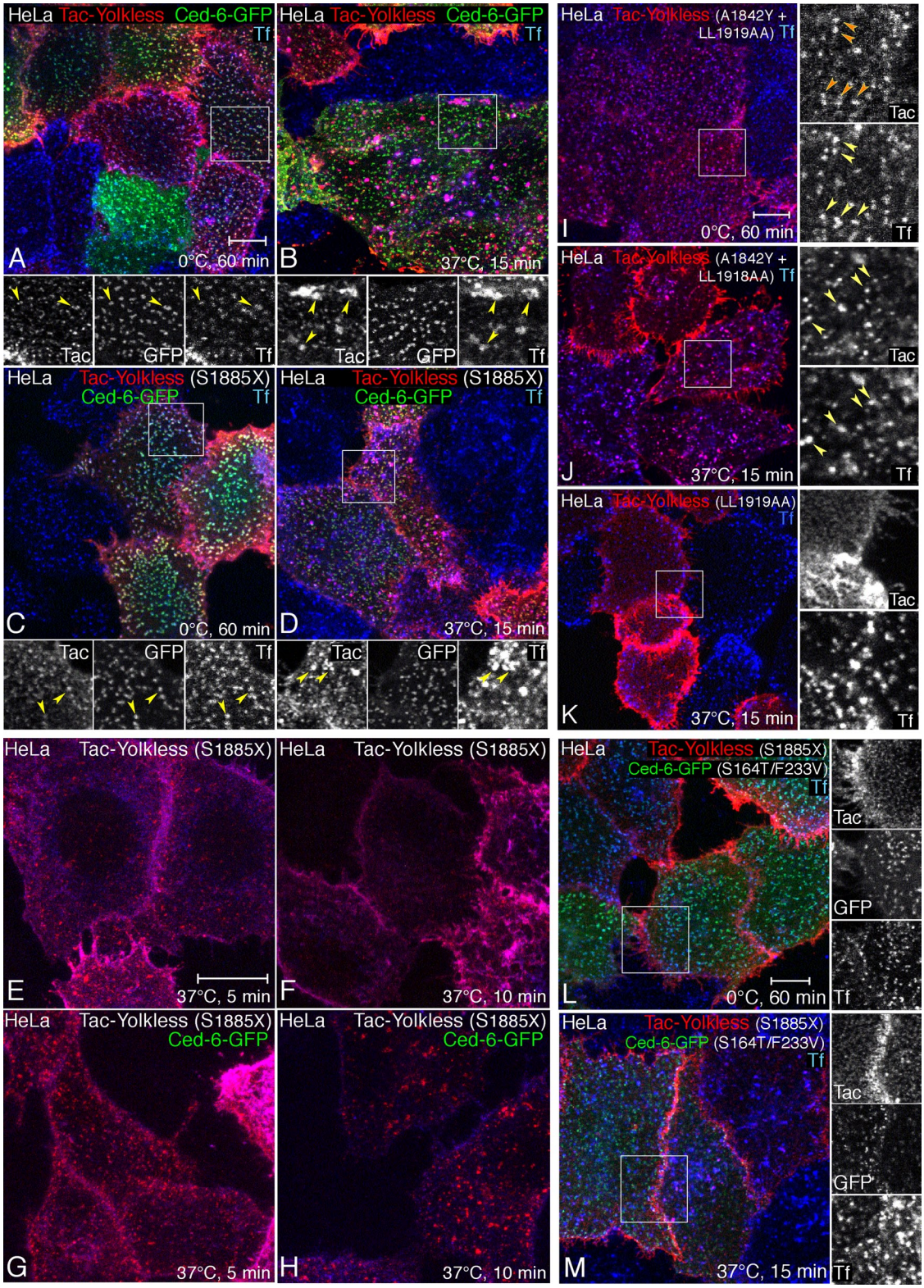

FIGURE 8: Ced-6 specifically recognizes the Yolkless FXNPXA signal. (A–D) HeLa cells transfected with Tac-Yolkless (A, B) or Tac-Yolkless (S1885X) (C, D) and Ced-6-GFP (green) were preincubated with a mixture of anti-Tac mAb and Alexa633 transferrin (blue) on ice. Washed cells were either fixed (A, C) or warmed to 37°C for 15 min and fixed (B, D), and then bound anti-Tac was visualized with an Alexa 568 anti-mouse antibody (red). Representative confocal optical sections are shown, with magnification of the boxed regions shown below. (E–H) Tac-Yolkless (S1885X) alone (E, F) or with Ced-6-GFP (G, H) transfected HeLa cells were preincubated with Alexa 546–conjugated anti-Tac on ice, washed, and warmed to 37°C for 5 or 10 min. Fixed cells were incubated with an Alexa 633–conjugated anti-mouse antibody without permeabilization. Confocal image stacks projected into a single maximal intensity image are shown. (I–K) HeLa cells transfected with Tac-Yolkless LL1919AA (K) or Tac-Yolkless (A1842Y/LL1919AA; I, J) were preincubated with a

fluorescent reporter. Although GULP has been localized to intracellular vesicular elements (Kiss *et al.*, 2006; Martins-Silva *et al.*, 2006; Beyer *et al.*, 2012), extensive colocalization with AP-2 and clathrin at the plasma membrane is entirely consistent with the coat protein–binding features seen in biochemical assays (Figure 3B); even presuming that the GULP PTB domain similarly engages PtdIns(4,5)P_2 and is known to bind to FXNPXY signals (Su *et al.*, 2002; Park *et al.*, 2008, 2010), these interactions alone will not place GULP physically in clathrin-coated structures at steady state (Mishra *et al.*, 2002a; Chetrit *et al.*, 2008).

Gulp (and Ced-6) has a wide expression pattern (Liu and Hengartner, 1999; Smits *et al.*, 1999; Hao *et al.*, 2011; Beyer *et al.*, 2012), but endogenous GULP is difficult to detect in HeLa cells (Hao *et al.*, 2011). Placenta is a source of many GULP ESTs and at least five cDNAs; a ~35-kDa protein, commonly detected by four independent anti-GULP antibodies, is present in placenta cytosol (Figure 9D). Of importance, GULP is strongly enriched in clathrin-coated vesicles purified from placenta (Figure 9D). The concentration of endogenous GULP parallels that of AP-2, Dab2, epsin 1, HIP1, and eps15—all authentic endocytic clathrin coat constituents. These biochemical data are fully consistent with the very recent proteomic cataloguing of GULP, together with AP-2 and clathrin, at the apical plasma membrane of placental syncytiotrophoblast (Vandre *et al.*, 2012). Coincidentally, the placental trophoblast plays a vital role in embryonic nutrient supply from the maternal circulation. Furthermore, the mammalian Gulp PTB domain binds physically to LRP1 (Kiss *et al.*, 2006), stabilin-2 (Park *et al.*, 2008), and amyloid precursor protein (Hao *et al.*, 2011; Beyer *et al.*, 2012)—all transmembrane proteins well established to undergo clathrin-dependent endocytosis (Li *et al.*, 2001; Thinakaran and Koo, 2008; Figure 10). However, in brain—also a source of Gulp transcripts (Liu and Hengartner, 1999; Martins-Silva *et al.*, 2006)—the protein is undetectable in either cytosol or coated vesicles.

Like *Drosophila* Ced-6, soluble placental GULP associates with both the α and β2 appendages of AP-2, although binding to the GST-α appendage shows a substantially higher apparent affinity compared with Ced-6 (Figure 9E). In the same experiment, endogenous Dab2 and eps15 within the placenta cytosol bind to the GST-α and -β2 appendages to a similar extent. Two different anti-GULP antibodies give similar results, and GULP-GFP, produced from a transgene in HeLa cells, also binds to the α appendage more efficiently than to the β2 appendage. Collectively our data argue that both Ced-6 and the chordate orthologue GULP fulfill the functional requirements for CLASP assignment. Furthermore, they suggest that Ced-6 has more numerous or distinct AP-2–binding motifs, which is consistent with the fly protein containing >200 additional amino acids.

DISCUSSION

Yolkless sorting and vitellogenesis

The recessive female sterile phenotype of *yolkless* mutants signifies the indispensable role of yolk accumulation in reproduction. However, although clathrin-mediated endocytosis was implicated early on in this process, the molecular descriptions of other important processes during *Drosophila* oogenesis, including stem cell division, symmetry breaking, cell polarity, directed mRNA positioning, and cytoskeletal dynamics, are more extensive and complete than that for vitellogenesis (Bastock and St Johnston, 2008). Yolk storage has many intriguing facets, however, that clearly distinguish it from standard clathrin-mediated endocytosis in cultured cell models. Remarkably, Yolkless appears to be the most important nutrient receptor for yolk accrual during vitellogenesis; the precipitous decline in morphologically discernible clathrin-coated structures at the oolemma of null females demonstrates the lynchpin activity of Yolkless in the egg chamber. Although lipophorin receptors are involved in lipid transport (Tufail and Takeda, 2009), recent data show that certain lipophorin receptors in *D. melanogaster* are not internalized efficiently, especially in the highly metabolically active germline nurse cells (Parra-Peralbo and Culi, 2011).

Yolkless has two functional endocytic sorting signals that engage different sorting machinery. An AP-2–dependent dileucine sequence is positioned near the C-terminus of the protein, and our results suggest that this signal is probably at least partly responsible for yolk uptake in a *ced-6*–deficient background. It is clear that AP-2 operates in clathrin-mediated endocytosis in the fly egg chamber. PtdIns(4,5)P_2 is required to dock AP-2 to the plasma membrane (Jackson *et al.*, 2010), and Skittles, a *Drosophila* type I phosphatidylinositol 4-phosphate 5-kinase, is expressed in the female germline (Hassan *et al.*, 1998; Compagnon *et al.*, 2009). In stage 9 hypomorphic *skittles* germline clones, clathrin-coated profiles at the oolemma are sharply reduced, bud morphology is grossly abnormal, and yolk accumulation is diminished (Compagnon *et al.*, 2009). More directly, immunoreactivity of the AP-2 α subunit is prominently cortical in vitellogenic cysts (Richard *et al.*, 2001; Dollar *et al.*, 2002; Sommer *et al.*, 2005; Compagnon *et al.*, 2009), and transgenic flies expressing the human transferrin receptor, which depends on a YTRF sorting signal (Collawn *et al.*, 1990) that is physically recognized by AP-2 (Ohno *et al.*, 1995; Motley *et al.*, 2003), internalize the ectopic receptor into the oocyte endosome compartment in a *shibire*-dependent manner (Bretscher, 1996). AP-2 is thus assembled in a sorting-competent conformation (Jackson *et al.*, 2010) to engage cargo at the oolemma of yolk-accumulating eggs.

Dileucine signals are also operative in *Drosophila*. A ^{1347}RSSQILL sequence in the Notch ligand Serrate promotes constitutive internalization (Glittenberg *et al.*, 2006). The atypical Yolkless dileucine (^{1914}AQEL**LL**E) does not exhibit the regular [DE]XXXLL-type spacing of upstream acidic residues, nor does it have a Pro preceding the first Leu to make it more effective (Kozik *et al.*, 2010). Trailing acidic side-chain pairs can also improve recognition of dileucine signals (Lindwasser *et al.*, 2008; Zhao *et al.*, 2008; Kozik *et al.*, 2010), and the single ^{1928}Asp resembles the positioning of the acidic Asp duo (+9 and +10 relative to the first Leu) in HIV Nef, which assists with AP-2 engagement (Lindwasser *et al.*, 2008; Chaudhuri *et al.*, 2009). The positioning of this acidic Yolkless residue, however, is not strictly conserved within the cytosolic domain of the evolutionarily closest Drosophilidae—*D. simulans, D. sechellia*, and *D. yakuba*. The B

mixture of anti-Tac mAb and Alexa 633 transferrin (blue) on ice. Washed cells were either fixed (I) or warmed to 37°C for 15 min and fixed (J, K), and then bound anti-Tac was visualized with an Alexa 568 anti-mouse antibody (red). Representative confocal optical sections are shown, with magnification of the boxed regions shown. (L, M) HeLa cells transfected with Tac-Yolkless (S1885X) and Ced-6-GFP (S164T/F233V; green) were preincubated with a mixture of anti-Tac mAb and Alexa 633 transferrin (blue) on ice. Washed cells were either fixed (L) or warmed to 37°C for 15 min and fixed (M), and then bound anti-Tac was visualized with an Alexa 568 anti-mouse antibody (red). Representative confocal optical sections are shown, with magnification of the boxed regions shown. Scale bar, 10 µm.

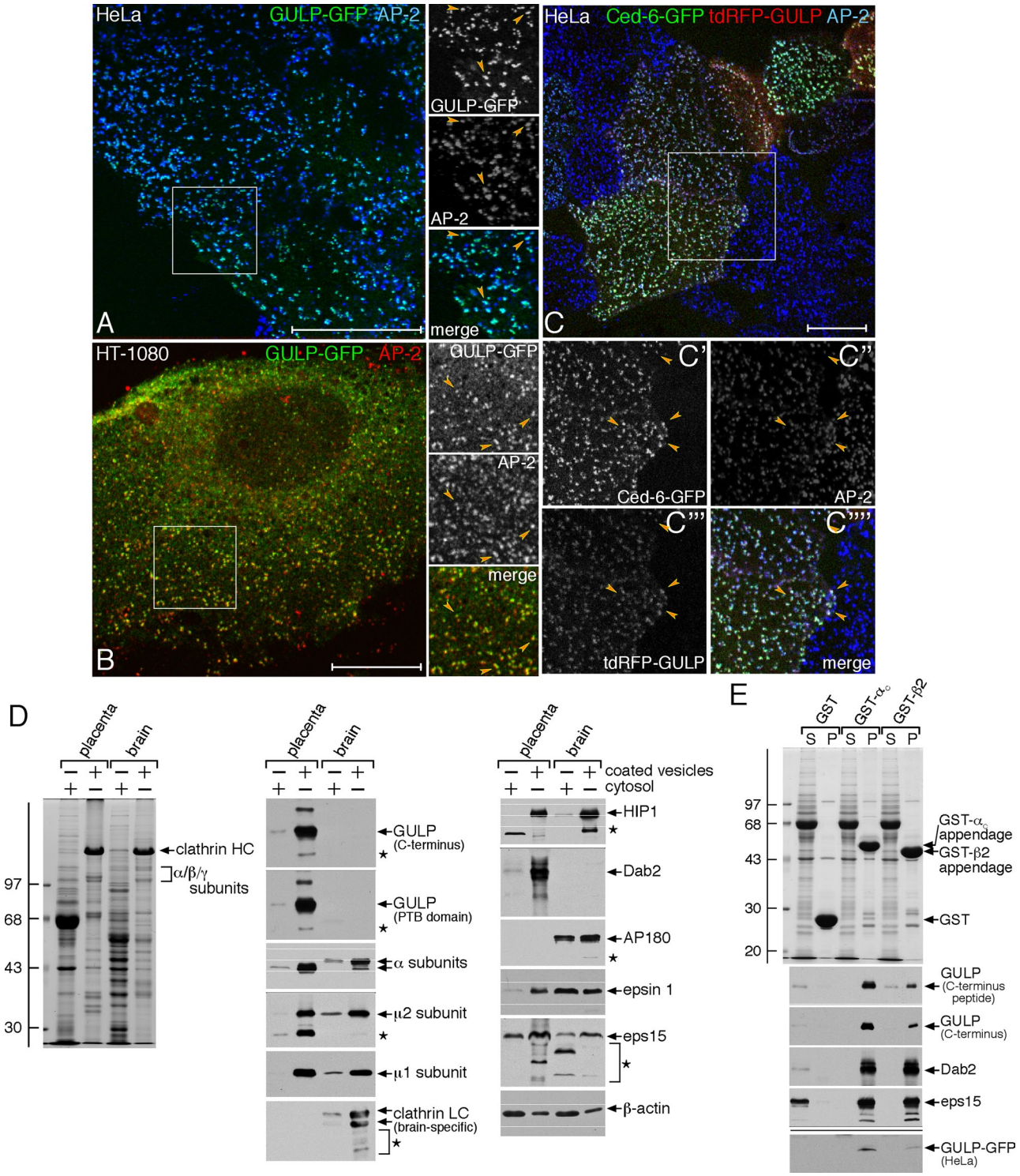

FIGURE 9: Vertebrate GULP is a CLASP. (A) Intracellular localization of transiently expressed GULP-GFP in fixed HeLa cells costained with an anti–AP-2 α subunit mAb (blue). A representative single confocal optical section is shown, with magnification of the boxed region below. Scale bar, 10 μm. Arrowheads, selected colocalization. (B) Colocalization of GULP-GFP with endogenous AP-2 in HT-1080 cells. (C) Overlap of transfected Ced-6-GFP and tdRFP-GULP with endogenous AP-2 in fixed HeLa cells. A representative image is shown, with magnified areas (below) corresponding to the box. (D) Equal aliquots of placenta or brain cytosol or purified placenta or brain clathrin-coated vesicles were resolved by SDS–PAGE and either stained or replicates immunoblotted using the indicated antibodies. Four independent anti-GULP antibodies gave analogous results; two are shown. Asterisks denote presumed degradation products. (E) Aliquots of S and P fractions from GST pull-down assays with the indicated GST fusion proteins and placental cytosol or GULP-GFP–transfected HeLa lysates were analyzed by SDS–PAGE with staining or immunoblot using the indicated antibodies; GULP-GFP was visualized with anti-GFP. The positions of the mass standards in kilodaltons are indicated.

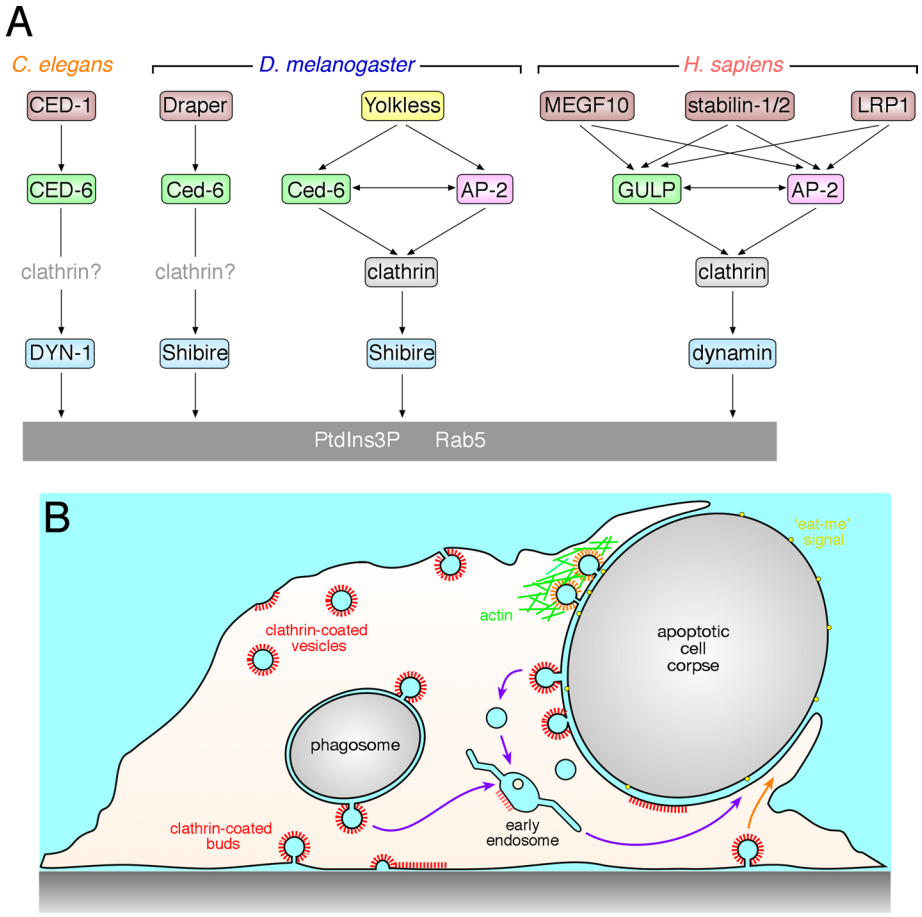

FIGURE 10: Mechanistic comparison of the endocytosis and phagocytosis pathways. (A) Diagrammatic representation of the relationship between Yolkless and phagocytic "eat me" signal receptors in selected invertebrates and humans. Linking arrows denote the relay of protein–protein interactions during endocytic uptake. The phagocytic receptors MEGF10 (Hamon *et al.*, 2006; Suzuki and Nakayama, 2007), stabilin-1/2 (Hansen *et al.*, 2005; Park *et al.*, 2008, 2010), and LRP1 (Su *et al.*, 2002) are tentatively implicated in apoptotic corpse engulfment in vertebrates. (B) Schematic hypothetical model for possible role(s) of clathrin-coated structures in the phagocytosis of apoptotic cell corpses. Assembled clathrin coats containing tyrosine-phosphorylated clathrin (orange bristles) linked to action polymerization (Bonazzi *et al.*, 2011) are distinguished from regular clathrin-coated structures (red bristles).

isoform of Yolkless has a 60-residue C terminus that replaces the 13-residue end of isoform A. The alternatively spliced B isoform has ^{1925}Glu that is favorably placed (at +7), and Yolkless proteins from some other *Drosophila* species have a Glu at position +6 or +8, which perhaps improves recognition by AP-2 (Kozik *et al.*, 2010). The crystal structure of the AP-2 core bound to dileucine internalization peptides shows that the predominant interaction involves placement of the two abutting Leu side chains into chemically compatible depressions, which are only accessible once AP-2 has undergone the conformational switch from the closed to the open state (Kelly *et al.*, 2008; Jackson *et al.*, 2010). Indeed, two adjacent Leu side chains alone can promote rather efficient uptake (Kozik *et al.*, 2010), and although there is a loose defining dileucine signal consensus sequence, there is much natural variation, perhaps reflecting limits of convergent evolution.

Even so, AP-2–null germline cysts still accumulate yolk (Parra-Peralbo and Culi, 2011), yet *clathrin*-null alleles cause a highly penetrant sterility (Bazinet *et al.*, 1993).Together, these apparently conflicting results show that although *yolkless* mutants have dramatically diminished numbers of clathrin-coated structures at the cortex (Schonbaum *et al.*, 2000; Sommer *et al.*, 2005), there must be operational clathrin coats in oocytes in which AP-2 genes have been deleted by directed recombination (Parra-Peralbo and Culi, 2011). This gross phenotype mirrors AP-2 siRNA in cultured cells and suggests that other, functionally redundant CLASPs can compensate for AP-2 loss in this recombined background. Our experiments indicate that Ced-6 fulfils this role functionally, that it is appropriately expressed and localized in vitellogenic oocytes, and that the PTB domain of *Drosophila* Ced-6 specifically engages both PtdIns(4,5)P_2 and the variant Yolkless FQNPLA signal, which is recognized poorly by the structurally related Dab2 or ARH PTB domains. In this regard, it is interesting that the longer *Drosophila* Ced-6 protein is more like Dab2 than ARH/trephin, with strong, multiple clathrin-binding sequences, which we predict still allow proper coat assembly and productive yolk uptake in an AP-2–compromised oocyte.

One reason for deploying numerous endocytic CLASPs is that the way in which membrane-tethered AP-2 recognizes sorting signals puts tight constraints on suitable positioning of the peptide ligands relative to the inner leaflet of the plasma membrane (Jackson *et al.*, 2010). Added CLASPs can accommodate, in addition to different peptide signals and posttranslational additions, internalization signals structured or oriented in a manner that is incompatible with AP-2 engagement. Another reason is that tandemly arrayed sorting signals within a receptor cytosolic domain can promote more rapid uptake than a solitary signal, in addition to making the internalization process more durable. The LDL receptor-related protein 1 (LRP1), for instance, displays a membrane-proximal NPXY signal, a second distal FXNPXY interleaved with a YXXØ signal (^{4502}**FTNPVYATL**), and two potential dileucine sequences (Li *et al.*, 2001). The kinetics of LRP1 uptake is considerably faster (~5- to 10-fold) than that of either the LDL or very low density lipoprotein (VLDL) receptor, but inactivation of the YXXØ signal diminishes the rate of internalization to that of the LDL and VLDL receptors, each of which depends on a single FXNPXY signal (Li *et al.*, 2001). Tandem endocytic sorting signals actually occur at high frequency in transmembrane proteins (Kozik *et al.*, 2010). The HIV env protein gp41 contains both GYXXØ and dileucine signals, and either can drive AP-2–dependent uptake (Byland *et al.*, 2007). During vitellogenic stages 8–12, the oocyte grows approximately four to five times faster than the nurse cells in the same egg chamber, and ~100-fold increase in the yolk volume occurs, from 7×10^4 to 8×10^6 μm^3 (King, 1970). After ~16 h of sustained endocytic activity, yolk bodies occupy up to ~33% of the cytoplasm of an oocyte (King, 1970). Avidity effects through multiple sorting signals and the participation of several independent, but functionally redundant clathrin adaptors likely underpin the dependability of this storage process by assuring maximal levels of cargo loading per bud cycle.

It is not yet established whether in *yolkless* mutant oocytes clathrin coats fail to form entirely or whether, more likely, a high incidence of abortive events makes ultrastructural identification of stable clathrin assemblages improbable. Proper incorporation of cargo is known to stabilize assembling coats and promote vectorial progression to the final fission step (Ehrlich *et al.*, 2004; Loerke *et al.*, 2009). We believe that the apparent density of clathrin coats decreases because of an abnormally high failure rate of assembly in the absence of Yolkless and, to a lesser extent, in *ced-6*–mutant egg chambers.

Ced-6/GULP in phagocytic engulfment

Strong genetic and functional evidence in *D. melanogaster* links Ced-6 to engulfment of apoptotic cell corpses, debris, and microorganisms (Awasaki *et al.*, 2006; MacDonald *et al.*, 2006; Cuttell *et al.*, 2008). Similarly, in *C. elegans* CED-6 operates with the "eat me" signal receptor CED-1 (Yu *et al.*, 2008; Figure 10) in a partially redundant pathway parallel to CED-2/CrkII, CED-5/Dock180, and CED-12/ELMO (Kinchen *et al.*, 2005), which is upstream of the actin-regulating small GTPase CED-10 (Rac). Invertebrate oocytes can be actively phagocytic and display some similarities with macrophages (Mishra, 2011). Ced-6 could conceivably then act in both endocytosis and phagocytosis in fly eggs, but the germline cysts of higher invertebrates are enveloped by a barrier somatic follicular epithelium. Egg development in *Drosophila* does involve apoptosis of nurse cells during late oogenesis, but this depends on lysosomes and autophagy and not phagocytosis (Bass *et al.*, 2009; Nezis *et al.*, 2010). After cytoplasmic dumping, degenerating nurse-cell remnants are excluded from incorporation into the mature oocyte by the vitelline membrane (King, 1970) and are engulfed by surrounding follicle cells (Nezis *et al.*, 2000). In addition, the apoptotic follicle cells in mature eggs are located outside of the egg case (Nezis *et al.*, 2002), and so there is no evidence that Ced-6 operates in a canonical phagocytic pathway in the fly oocyte. Instead, the vertebrate Ced-6 orthologue GULP, despite sequence divergence, displays analogous, evolutionarily retained interactions with primary clathrin coat constituents. This suggests that a fundamental mode of operation is conserved in chordates and provides the first evidence that the precise mode of action of Ced-6/GULP may be different from current paradigms (Zhou and Yu, 2008; Lu and Zhou, 2012; Kinchen, 2010). Intriguingly, phagocytosis of *Escherichia coli* by *Drosophila* S2 cells is diminished >80% by clathrin RNA interference (RNAi; Rocha *et al.*, 2011).

In worms, CED-1 (with putative ^{960}FQNPLY, ^{1019}YASL, and ^{1085}YADI sorting signals) concentrates on the plasma membrane site of phagocytosis and is enriched in the nascent phagosome (Yu *et al.*, 2008). DYN-1 (dynamin) is required in engulfing cells for dead cell uptake and operates in the CED-1 pathway after CED-6 (Yu *et al.*, 2006; Figure 10A). The precise interplay between CED-1, CED-6, dynamin, and phagocytosis remains to be established. What is certain is that CED-1 and DYN-1 exit the maturing phagosome early (5–10 min), long before degradation of an apoptotic corpse (~60 min; Yu *et al.*, 2006, 2008; Chen *et al.*, 2010). DYN-1 apparently operates both early, in promoting physical engulfment, and later, in phagosome maturation (Yu *et al.*, 2006; Lu and Zhou, 2012). Given that Ced-6 interfaces with the core clathrin coat, our results provide an alternate explanation for how DYN-1 operates initially in a genetic pathway downstream of CED-6 (Yu *et al.*, 2006). The *dyn-1* mutants display a defect in pseudopod extension (Yu *et al.*, 2006), and so the involvement of Ced-6 in engulfment of apoptotic cell corpses could (in part) be to recycle CED-1 locally for timely extension of large pseudopods over a sizable cell corpse. The data also seem to be consistent with defective CED-6–dependent, clathrin-mediated endocytosis at the phagocytic cup (Figure 10B). Indeed, years ago, electron microscopy studies revealed extensive clathrin-coated membrane and buds connected to forming phagocytic cups (Aggeler and Werb, 1982).

Removal of apoptotic corpses in flies requires tyrosine kinase and Ca^{2+}-channel signaling downstream of the "eat me" signal receptor Draper (Cuttell *et al.*, 2008; Ziegenfuss *et al.*, 2008). Thus, it is also possible that these signal inputs change the basal activity of Ced-6 to facilitate engulfment-specific operations. For example, Src-modified clathrin is linked to sites of bacterial internalization (Bonazzi *et al.*, 2011). In cell infection models, cooperation between tyrosine-phosphorylated clathrin, Dab2 (a Ced-6–related PTB-domain clathrin adaptor), and Hip1R, an actin-binding protein that also engages clathrin directly (Engqvist-Goldstein *et al.*, 2001; Brett *et al.*, 2006; Wilbur *et al.*, 2008), leads to the formation of actin-rich platforms functionally linked to bacterial invasion/pathogenesis (Pizarro-Cerda *et al.*, 2010; Bonazzi *et al.*, 2011). It is hypothesized that phosphorylated clathrin stabilizes clathrin-coated structures to nucleate local actin assembly while also providing a cluster of mature, coated buds for swift internalization immediately upon dephosphorylation (Bonazzi *et al.*, 2011). This may be mechanistically advantageous during phagocytosis, and Ced-6 could conceivably operate in an analogous manner to Dab2 at the nascent phagocytic cup (Figure 10B). Finally, two other clathrin/dynamin-associated endocytic proteins have recently been linked genetically to phagocytic uptake of apoptotic cell corpses in *C. elegans*. Both sorting nexin 9 (SNX-9/LST-4; Almendinger *et al.*, 2011; Lu *et al.*, 2011) and PIKI-1, a class II PtdIns(4,5)P_2 3-kinase (Lu *et al.*, 2012), promote uptake of cellular debris upstream of RAB-5. The orthologous proteins in mammals bind physically to clathrin (Gaidarov *et al.*, 2001; Lundmark and Carlsson, 2003; Miele *et al.*, 2004). Clathrin could conceivably be involved in coordinating a molecular scaffold for selective phosphoinositide remodeling during phagocytosis. Although further experimentation is certainly required to clarify the precise mechanistic link between Ced-6 and clathrin during phagocytosis, the conventional CLASP activity of Ced-6 in yolk endocytosis justifies the effort.

MATERIALS AND METHODS

DNA, RNA, and molecular cloning

The cDNAs encoding *Drosophila* Ced-6 (GenBank AY119596), RAP (AY051766), and Yolkless (BT003478) were from the *Drosophila* Genomics Resource Center at the University of Indiana (Bloomington, IN). The receptor-associated protein (RAP) fusion protein was generated by insertion of the *Drosophila* RAP cDNA (GenBank clone AY051766) lacking the N-terminal signal sequence into pGEX-4T-1–mcRFP (Shaner *et al.*, 2004) to create a tandem GST-mcRFP-RAP fusion. A GFP-*Drosophila* clathrin light-chain plasmid, kindly supplied by Henry Chang (Chang *et al.*, 2002), was used to generate transgenic flies by insertion of PCR-amplified GFP-clathrin light-chain sequence into pUASp (Rorth, 1998) for germline expression. The Ced-6 whole-mount in situ probe was prepared by PCR using GenBank clone AY119596 as template with 5′-CGACACCAATTCCACCACAG-3′ forward and 5′-GCGTAATACGACTCACTATAGGGAGGATCCAAACTCTCCAGCG-3′ reverse primers. The reverse primer incorporates a T7 RNA polymerase promoter sequence (underscored) for antisense riboprobe synthesis as described previously (Mishra *et al.*, 2008) and was used for the synthesis of digoxigenin (DIG)-labeled probes with a digoxigenin-11 UTP RNA labeling mix (Roche, Indianapolis, IN). The same template was used to clone full-length Ced-6 (residues 1–517) into pGEX-4T-1, pET28, and pEGFP-N1 vectors and truncations and mutants (GST-Ced-6 1–300; 285–517; 370–517; 401–517; 430–517; 401–468; 401–500; 475–517; 475–500; 493–517; DPF → APA; or the S164T/F233V compound

mutant) prepared either by PCR or by introduction of appropriate stop codons/nucleotide base changes using QuikChange mutagenesis (Stratagene/Agilent Technologies, Santa Clara, CA). The *B. mori* Ced-6 orthologue cDNA (clone fufe47K07) was kindly supplied by Kazuei Mita (Ishii *et al.*, 2010) and similarly cloned by PCR into pGEX-4T-1. GULP-GFP was kindly provided by Scott Kiss and Ravi Ravichandran (Kiss *et al.*, 2006). The tdRFP-GULP was generated by PCR using GenBank clone BC068525 as the template with ligation of the digested PCR amplicon into the tdRFP plasmid (Keyel *et al.*, 2008). Plasmids encoding the GST–AP-2 α_C (Traub *et al.*, 1999) and β2 appendages (Edeling *et al.*, 2006; Thieman *et al.*, 2009) and appropriate mutants have been described.

Tac in pcDNA3.1 (Hawryluk *et al.*, 2006) was used as the ectopically expressed transmembrane protein control. The cytosolic domain of Yolkless (residues 1829–1937) was PCR amplified from GenBank clone BT003478 and inserted into the Tac plasmid to replace the endogenous Tac cytosolic segment. The same region of Yolkless was subcloned into pET28. Site-directed mutants (S1885X, LL1919AA, and A1842Y) were generated using the QuikChange procedure.

All constructs were verified by automated dideoxynucleotide sequencing (Genewiz, South Plainfield, NJ), and the primer and restriction-site details, sequences, and maps are all available upon request. The siRNA oligonucleotide duplexes (Dharmacon, Lafayette, CO) for gene silencing of the AP-2 α subunit and clathrin heavy-chain transcripts have been described (Keyel *et al.*, 2006, 2008).

Antibodies

The rat anti–Ced-6 serum was generously provided by Takeshi Awasaki (Awasaki *et al.*, 2006). The affinity-purified rat anti-Yolkless antibodies were kindly provided by Anthony Mahowald (Schonbaum *et al.*, 2000), the rabbit anti-*Drosophila* YP1-3 was kindly provided by Mary Bownes (Bownes *et al.*, 2002), polyclonal rabbit anti-μ2 subunit and anti-Tac antisera were kindly provided by Juan Bonifacino, the affinity-purified rabbit anti-GULP PTB domain was kindly provided by Ravi Ravichandran (Ma *et al.*, 2007), the affinity-purified rat anti-GULP was kindly provided by K.-F. Lau (Hao *et al.*, 2011), and the affinity-purified rabbit anti-GFP was kindly provided by Phyllis Hanson (Dalal *et al.*, 2004). The anti–clathrin heavy chain mAb TD.1 (Nathke *et al.*, 1992) and anti–AP-2 α subunit mAb AP.6 (Chin *et al.*, 1989) were kindly provided by Frances Brodsky, the anti-clathrin light chain mAb CI57.3 was kindly provided by Reinhard Jahn, and the guinea pig anti-Liquid facets (epsin) serum was kindly provided by Bing Zhang.

We described previously the production and use of affinity-purified rabbit anti-Dab2 (Mishra *et al.*, 2002a), anti–epsin 1 (Drake *et al.*, 2000), anti-HIP1 (Mishra *et al.*, 2001), anti–AP-1/AP-2 β1/β2 subunit (GD/1), and anti-μ1 subunit (RY/1) (Traub *et al.*, 1995) antibodies. An affinity-purified anti-AP180 antibody (LV/1) was prepared similarly from rabbit immune serum using the immunizing peptide (LVGNLGISGTTSKKGDL) coupled to CNBr-activated Sepharose CL-4B (GE Healthcare, Piscataway, NJ).

Commercial antibodies used were as follows: rabbit anti-eps15 and anti-actin mAb C4 (Santa Cruz Biotechnology, Santa Cruz, CA), anti–AP-2 α subunit mAb clone 8 (BD Transduction Laboratories, Lexington, KY), peptide affinity–purified rabbit (GeneTex, Irvine, CA) or goat (Imgenex, San Diego, CA) anti-GULP C-terminus, and anti-Tac (CD25) mAb 7G7B6 from Ancell (North Bayport, MN) or affinity-purified rabbit anti-Tac (Cell Signaling Technology, Beverly, MA). The Alexa-conjugated anti-Tac mAb was prepared using mAb 7G7B6 with an Alexa Fluor 546 monoclonal antibody labeling kit as recommended by the manufacturer (Invitrogen, Carlsbad, CA). The anti–β-tubulin mAb E7 was purchased from the Developmental Studies Hybridoma Bank (University of Iowa, Iowa City, IA). Various Alexa-conjugated anti-mouse, -rabbit, -guinea pig, and -rat secondary antibodies were obtained from Invitrogen, and Cy5-conjugated antibodies for fluorescence and horseradish peroxidase–conjugated secondary antibodies for immunoblotting were purchased from GE Healthcare. The alkaline phosphatase–conjugated sheep anti-DIG for in situ analysis was from Roche (Indianapolis, IN).

Fly procedures

The wild-type strain was Canton-S. pUASp-*clc* transgenic lines were generated by BestGene (Chino Hills, CA) and crossed with the germline maternal GAL4 triple driver line (Lee and Cooley, 2007) for oocyte expression. The *yolkless* (y^1, cv^1, v^1, yl^{15}, f^1/*FM0*; strain 4612; DiMario and Mahowald, 1987) was from the Bloomington *Drosophila* Stock Center (Indiana University, Bloomington, IN), and the *ced-6* strain (*w*; *ced-6*^{J26}/*CyO*, *Act-GFP*) was generously provided by Takeshi Awasaki (Hashimoto *et al.*, 2009; Kuraishi *et al.*, 2009). Unless indicated, flies were typically maintained at 26.5°C on standard cornmeal molasses medium with added yeast paste. Reproductive diapause was induced experimentally by shifting vials of *D. melanogaster* (Canton-S) to 11°C with a 14-h dark cycle for 72 h. This was followed by further 36 h under the same conditions (diapause × 2) or a parallel shift to room temperature (release). Ovaries were dissected at room temperature in either Schneider's *Drosophila* medium (Life Technologies, Carlsbad, CA) or phosphate-buffered saline (PBS). Pools of whole dissected ovaries from females subjected to the indicated treatments were solubilized in SDS sample buffer for total protein analysis by SDS–PAGE. Incubation with the trypan blue (0.04% in PBS) or thrombin-cleaved mcRFP-RAP (0.16 mg/ml in PBS) endocytic tracers was at room temperature for 20 min. After washing in PBS, ovaries were fixed in 4% paraformaldehyde (Electron Microscopy Sciences, Hatfield, PA) for 30 min. For hemolymph collection, the abdomens of six yeast paste–fed females were pierced with a tungsten needle while they were immersed in a single drop of 100 µl of PBS on a sheet of Parafilm (DiMario and Mahowald, 1987). After 5 min at room temperature, the PBS was quantitatively aspirated and transferred to a microfuge tube. Protein in the hemolymph extracts was precipitated with methanol/chloroform (Wessel and Flugge, 1984) and each air-dried pellet was resuspended in 40 µl of SDS sample buffer. Fertility studies involved placing replicates of five *ced-6*^{J26}/CyO heterozygous or five *ced-6*^{J26} homozygous females into fresh vials each containing three Canton-S males. After incubation at 26.5°C for 14 d, the total number of adult flies/vial was determined.

Cell culture

HeLa SS6 (Elbashir *et al.*, 2001) and HT-1080 (Rasheed *et al.*, 1974) cells were passaged by trypsinization into DMEM supplemented with 10% fetal calf serum and 2 mM L-glutamine. Growth was at 37°C in a humidified 5% CO_2 incubator. Cells were routinely plated onto round, glass coverslips prior to transfection with Lipofectamine 2000 (Invitrogen) as described previously (Hawryluk *et al.*, 2006; Keyel *et al.*, 2006, 2008; Pedersen *et al.*, 2010), normally using 500 ng of endotoxin-free plasmid DNA per 35-mm dish or well of a six-well tray. For AP-2 α subunit and clathrin heavy-chain siRNA, cells were silenced twice, the cells being replated 24 h after first transfection using Oligofectamine (Invitrogen). RNAi-treated cells were transfected 6 h later with Tac-Yolkless using Lipofectamine 2000 and analyzed after ~10–15 h at 37°C. For calyculin treatment, Ced-6-GFP–transfected cells in 35-mm dishes were incubated in

the presence or absence of 100 nM calyculin A (LC Laboratories, Woburn, MA) at 37°C for 60 min. All washing and trypsinization solutions for the inhibitor-treated cells contained 100 nM calyculin A, and detached cells were washed by centrifugation (500 × g_{max}, 4°C, 5 min) and solubilized in SDS sample buffer.

Surface biotinylation and endocytosis assays

Transiently transfected HeLa cells cultured in six-well trays were used for biotinylation with sulfo-NHS-SS-biotin (Thermo Scientific, Waltham, MA). After washing with Ca^{2+}- and Mg^{2+}-supplemented PBS (PBS^{++}), the monolayers were surface biotinylated twice with 1 mM sulfo-NHS-SS-biotin in PBS^{++} on ice for 30 min. The cells were then quenched with 50 mM glycine and 0.5% bovine serum albumin (BSA) in PBS^{++}, washed with PBS^{++}, and then either retained on ice or incubated in a 37°C water bath for 5–20 min. Cells were chilled on ice and washed rapidly with ice-cold PBS^{++}, and then surface-exposed biotin was removed with two sequential incubations in 50 mM reduced glutathione, 75 mM NaCl, 75 mM NaOH, 1.25 mM $CaCl_2$, 1.25 mM $MgSO_4$, and 0.2% BSA, pH 8.5, for 30 min on ice. After aspiration of the glutathione cleavage buffer, the cell monolayers were incubated in 50 mM iodoacetamide in PBS^{++} for 30 min, washed twice with ice-cold PBS^{++}, and lysed. The lysis buffer contained 25 mM 4-(2-hydroxyethyl)-1-piperazineethanesulfonic acid (HEPES)–KOH, pH 7.2, 125 mM potassium acetate, 5 mM magnesium acetate, 2 mM ethylene glycol tetraacetic acid (EGTA), 2 mM EDTA (assay buffer) supplemented with 1% (wt/vol) Triton X-100, 2.5 mM iodoacetamide, 0.5 mM phenylmethylsulfonyl fluoride (PMSF), and Complete Protease Inhibitor Cocktail (Roche) and was incubated with cells for 30 min on ice before scraping up cell remnants and transferring to microfuge tubes on ice. After centrifugation (10,000 × g_{max}, 4°C, 10 min) each soluble lysate was transferred to a new tube and incubated with ~25 µl of packed NeutrAvidin agarose (Thermo Scientific) for 2 h at 4°C. After sedimentation and washing, proteins bound to the agarose were solubilized in SDS sample buffer and boiled before SDS–PAGE analysis and immunoblotting.

Protein purification and biochemistry

Recombinant GST and GST- and hexahistidine (His_6)-tagged proteins were produced in *E. coli* by standard procedures after induction with 100 µM isopropyl-β-D-thiogalactoside at room temperature (Traub *et al.*, 1999; Drake and Traub, 2001). GST-fusion proteins were routinely eluted from glutathione-Sepharose 4B (GE Healthcare) with 10 mM reduced glutathione and dialyzed into PBS at 4°C before use. The purified recombinant AP-2 core complex was a generous gift from David Owen (University of Cambridge). High-speed rat brain cytosol was prepared from crude homogenates by sequential differential centrifugation using a buffer of 25 mM HEPES-KOH, pH 7.2, 250 mM sucrose, 2 mM EDTA, 2 mM EGTA, and 1 mM PMSF with added Complete Protease Inhibitor Cocktail. Preparation of clathrin-coated vesicles from frozen brain tissue (Pel-Freez Biologicals, Rogers, AR) used the standard 12.5% Ficoll/12.5% sucrose differential centrifugation procedure (Campbell *et al.*, 1984) and has been described (Mishra *et al.*, 2001). Similar preparation of placenta cytosol and purified placental clathrin-coated vesicles has been detailed (Hawryluk *et al.*, 2006). Preparative lysates from transfected HeLa cells were made using in assay buffer supplemented with 1 mM dithiothreitol (DTT), 1% Triton X-100, 1 mM PMSF, and Complete Protease Inhibitor Cocktail. Following cell solubilization on ice for 30 min, lysate was prepared by centrifugation (20,000 × g_{max}, 4°C, 20 min) and aliquots stored at –80°C before use.

The synthetic multilamellar liposome stocks composed of 10% (wt/vol) cholesterol, 35% PtdCho, 35% PtdEth, 10% PtdSer, and 10% of either PtdIns or PtdIns(4,5)P_2 were prepared at a concentration of 4 mg/ml and stored at –80°C before use. Phospholipid-binding assays (200-µl final volume) contained 0.4 mg/ml synthetic liposomes, 25–100 µg/ml thrombin-cleaved PTB domain, and 100 µg/ml BSA in assay buffer (Mishra *et al.*, 2002a). After incubation on ice for 30 min, liposomes were sedimented (20,000 × g_{max}, 4°C, 15 min) and aliquots of the supernatant and resuspended pellet fractions analyzed by SDS–PAGE.

Protein–protein interaction assays were performed using immobilized GST- or His_6-fusion proteins as described (Mishra *et al.*, 2001, 2002a, 2005, 2008; Jha *et al.*, 2004; Hawryluk *et al.*, 2006). Samples of 5–200 µg of the indicated protein were immobilized on ~25 µl of packed glutathione-Sepharose 4B or nickel–nitriloacetic acid–agarose and washed before use in pull-down assays. Soluble extracts were clarified by centrifugation to remove particulate material before adding to the beads. Assays were routinely performed in assay buffer supplemented with 1 mM DTT in a final volume of 350 µl and incubated at 4°C for 60 min. Tubes were centrifuged (10,000 × g_{max}, 4°C, 1 min) and an aliquot of the supernatant fraction collected. After washing of the beads four times with ice-cold PBS, the pellets were resuspended in SDS sample buffer. Typically, aliquots corresponding to 2% of the supernatant fraction and 12.5% of the resuspended pellet were analyzed by SDS–PAGE and immunoblotting. Binary protein–protein interaction assays were supplemented with 0.1 mg/ml BSA as a carrier.

SDS–PAGE and immunoblotting

Samples boiled in reducing SDS sample buffer were resolved on by SDS–PAGE on gels prepared from a 30:0.4 acryamide:bisacrylamide stock to improve resolution. Gels were either stained in Coomassie blue in 40% methanol, 10% acetic acid or transferred to nitrocellulose in 15.6 mM Tris, 120 mM glycine without methanol. After staining with Ponceau S, marked blots were blocked with 5% skim milk in 10 mM Tris-HCl, pH 7.8, 150 mM NaCl, and 0.1% Tween 20 and incubated with antibodies by standard procedures. Detection with horseradish peroxidase–labeled secondary antibodies was with HyGLO enhanced chemiluminscence (Denville Scientific, Metuchen, NJ).

Tissue and cell staining

Whole-mount in situ hybridization was performed as described in detail previously for *A. aegypti* egg chambers (Mishra *et al.*, 2008). Ovaries were fixed overnight in 4% paraformaldehyde and stored at –20°C in methanol before use. After hybridization and incubation with the anti-DIG antibodies, ovaries were washed extensively and the color reaction performed in the presence of 5-bromo-4-chloro-3′-indolyphosphate *p*-toluidine and nitro-blue tetrazolium.

For immunofluorescence analysis of dissected ovaries, paraformaldehyde-fixed samples were washed in PBS and then incubated in 2% BSA, 5% normal goat serum, and 0.3% Triton X-100 at room temperature for 30 min. Washed ovaries were then incubated with primary antibodies overnight at 4°C and with fluorophore-conjugated secondary antibodies at room temperature for 60 min. Where indicated, Alexa 488–phalloidin (1:500; Molecular Probes, Invitrogen) was added for 60 min and/or Hoechst 33258 (2 µg/ml in PBS) used to counterstain nuclei. Ovaries were mounted in Gelvatol.

Cultured cell analysis was typically done ~10–15 h after transfection. For assays following transferrin internalization, cells were preincubated at 37°C for 60 min in DMEM supplemented with 25 mM HEPES-KOH, pH 7.2, and 0.5% BSA to discharge prebound transferrin. The medium was replaced; cells were chilled on ice and then

incubated with either anti-Tac mAb or a mixture of the anti-Tac mAb and 25 µg/ml of the appropriate Alexa-conjugated transferrin for 60 min. The culture medium was rapidly aspirated and replaced with warmed medium, followed by incubation in a 37°C water bath for 2–25 min. Internalization was terminated by placing cells on ice and washing with ice-cold PBS before fixation in 4% paraformaldehyde. Control cells were fixed after washing without warming.

Microscopy and imaging

For electron microscopy, dissected *Drosophila* Canton-S ovaries were fixed in 2.5% glutaraldehyde in PBS for 10 min at room temperature. Samples were stained in 1% osmium tetroxide and 1% potassium ferricyanide for 1 h before dehydration in ethanol and embedding in Epon resin. Thin sections were stained with uranyl acetate and lead citrate. Sections were examined by transmission electron microscopy (JEOL 1210; JEOL, Peabody, MA) and images collected with an ATM digital camera.

Intact flies were anesthetized with FlyNap (Carolina Biological Supply, Burlington, NC) prior to photography with a Zeiss Discovery V8 dissecting microscope (Carl Zeiss, Jena, Germany) equipped with a Jenoptik ProgRes C5 camera (Jenoptik, Jena Germany). For microscopy of whole mount in situ, dissected ovarioles were equilibrated in 50% glycerol in PBS.

All confocal imaging was performed with an inverted Olympus FluoView FV1000 instrument (Olympus, Center Valley, PA) using sequential line scanning. An argon laser for 488-nm excitation and two helium–neon lasers for 543- and 633-nm excitation were used through a PlanApomat 60×, 1.40 numerical aperture objective with a 488/543/633 dichroic. The emitted light signal was separated with SDM560 and SDM640 beam splitters and passed through either bandpass filters BA505–525 (green), BA560–600 (red), and long-pass filter BA660IF (Cy5) or diffraction gratings that pass 500- to 530-nm (green) or 555- to 625-nm (red) light or a BA650IF filter (Cy5) before detection. Cropping and minor adjustments to the contrast or brightness of digital TIFF image files were performed with Photoshop CS4 (Adobe, San Jose, CA) and the composite images assembled with Freehand FX (Macromedia, Adobe) or Illustrator CS4 (Adobe).

ACKNOWLEDGMENTS

We are especially grateful to Takeshi Awasaki for most generously providing the Ced-6 reagents, to Sanjay Mishra for his contribution to the early stages of this project, to Becky Hughey for advice on surface biotinylation, to Juan Bonifacino, Mary Bownes, Henry Chang, Lynn Cooley, Robert Kiss, K.-F. Lau, Anthony Mahowald, Kazuei Mita, David Owen, Kodi (Ravi) Ravichandran, and Bing Zhang providing important materials and fly stocks, and to Yang Hong, John (Nick) Johnson, David Owen, and Ernst Ungewickell for critical discussion and advice. This work was supported by National Institute of Health Grant R01 DK53249.

REFERENCES

Aggeler J, Werb Z (1982). Initial events during phagocytosis by macrophages viewed from outside and inside the cell: membrane-particle interactions and clathrin. J Cell Biol 94, 613–263.

Almendinger J, Doukoumetzidis K, Kinchen JM, Kaech A, Ravichandran KS, Hengartner MO (2011). A conserved role for SNX9-family members in the regulation of phagosome maturation during engulfment of apoptotic cells. PLoS One 6, e18325.

Anderson E (1964). Oocyte differentiation and vitellogenesis in the roach *Periplaneta americana*. J Cell Biol 20, 131–155.

Anderson WA, Spielman A (1971). Permeability of the ovarian follicle of *Aedes aegypti* mosquitoes. J Cell Biol 50, 201–221.

Atella GC, Silva-Neto MA, Golodne DM, Arefin S, Shahabuddin M (2006). *Anopheles gambiae* lipophorin: characterization and role in lipid transport to developing oocyte. Insect Biochem Mol Biol 36, 375–386.

Awasaki T, Tatsumi R, Takahashi K, Arai K, Nakanishi Y, Ueda R, Ito K (2006). Essential role of the apoptotic cell engulfment genes draper and ced-6 in programmed axon pruning during *Drosophila* metamorphosis. Neuron 50, 855–867.

Bakken AH (1973). A cytological and genetic study of oogenesis in *Drosophila melanogaster*. Dev Biol 33, 100–122.

Banks SM, Cho B, Eun SH, Lee JH, Windler SL, Xie X, Bilder D, Fischer JA (2011). The functions of auxilin and rab11 in *Drosophila* suggest that the fundamental role of ligand endocytosis in notch signaling cells is not recycling. PLoS One 6, e18259.

Bass BP, Tanner EA, Mateos San Martin D, Blute T, Kinser RD, Dolph PJ, McCall K (2009). Cell-autonomous requirement for DNaseII in nonapoptotic cell death. Cell Death Differ 16, 1362–1371.

Bastock R, St Johnston D (2008). *Drosophila* oogenesis. Curr Biol 18, R1082–R1087.

Bazinet C, Katzen AL, Morgan M, Mahowald AP, Lemmon SK (1993). The *Drosophila* clathrin heavy chain gene: clathrin function is essential in a multicellular organism. Genetics 134, 1119–1134.

Beyer AS *et al.* (2012). Engulfment adapter PTB domain containing 1 interacts with and affects processing of the amyloid-β precursor protein. Neurobiol Aging 33, 732–743.

Bilder D, Haigo SL (2012). Expanding the morphogenetic repertoire: perspectives from the *Drosophila* egg. Dev Cell 22, 12–23.

Bodenmiller B *et al.* (2007). PhosphoPep—a phosphoproteome resource for systems biology research in *Drosophila* Kc167 cells. Mol Syst Biol 3, 139.

Bonazzi M *et al.* (2011). Clathrin phosphorylation is required for actin recruitment at sites of bacterial adhesion and internalization. J Cell Biol 195, 525–536.

Bownes M, Hurd H, Busgen T, Servay D, Alvis S, Popovic B, Bruce S, Burns I, Rothwell K, Walkinshaw M (2002). *Drosophila* yolk protein produced in *E. coli* is accumulated by mosquito ovaries. Insect Mol Biol 11, 487–496.

Bretscher MS (1996). Expression and changing distribution of the human transferrin receptor in developing *Drosophila* oocytes and embryos. J Cell Sci 109, 3113–3119.

Brett TJ, Legendre-Guillemin V, McPherson PS, Fremont DH (2006). Structural definition of the F-actin-binding THATCH domain from HIP1R. Nat Struct Mol Biol 13, 121–130.

Bu G (2001). The roles of receptor-associated protein (RAP) as a molecular chaperone for members of the LDL receptor family. Int Rev Cytol 209, 79–116.

Byland R, Vance PJ, Hoxie JA, Marsh M (2007). A conserved dileucine motif mediates clathrin and AP-2-dependent endocytosis of the HIV-1 envelope protein. Mol Biol Cell 18, 414–425.

Campbell C, Squicciarini J, Shia M, Pilch PF, Fine RE (1984). Identification of a protein kinase as an intrinsic component of rat liver coated vesicles. Biochemistry 23, 4420–4426.

Chang HC, Newmyer SL, Hull MJ, Ebersold M, Schmid SL, Mellman I (2002). Hsc70 is required for endocytosis and clathrin function in *Drosophila*. J Cell Biol 159, 477–487.

Chaudhuri R, Mattera R, Lindwasser OW, Robinson MS, Bonifacino JS (2009). A basic patch on α-adaptin required for binding of HIV-1 Nef and cooperative assembly of a CD4-Nef-AP-2 complex. J Virol 83, 2518–2530.

Chen D, Xiao H, Zhang K, Wang B, Gao Z, Jian Y, Qi X, Sun J, Miao L, Yang C (2010). Retromer is required for apoptotic cell clearance by phagocytic receptor recycling. Science 327, 1261–1264.

Chen WJ, Goldstein JL, Brown MS (1990). NPXY, a sequence often found in cytoplasmic tails, is required for coated pit-mediated internalization of the low density lipoprotein receptor. J Biol Chem 265, 3116–3123.

Chetrit D, Ziv N, Ehrlich M (2008). Dab2 regulates clathrin assembly and cell spreading. Biochem J 418, 701–715.

Chin DJ, Straubinger RM, Acton S, Nathke I, Brodsky FM (1989). 100-kDa polypeptides in peripheral clathrin-coated vesicles are required for receptor-mediated endocytosis. Proc Natl Acad Sci USA 86, 9289–9293.

Chintapalli VR, Wang J, Dow JA (2007). Using FlyAtlas to identify better *Drosophila* melanogaster models of human disease. Nat Genet 39, 715–720.

Cho KH, Raikhel AS (2001). Organization and developmental expression of the mosquito vitellogenin receptor gene. Insect Mol Biol 10, 465–474.

Clark AG *et al.* (2007). Evolution of genes and genomes on the *Drosophila* phylogeny. Nature 450, 203–218.

Collawn JF, Stangel M, Kuhn LA, Esekogwu V, Jing SQ, Trowbridge IS, Tainer JA (1990). Transferrin receptor internalization sequence YXRF implicates a tight turn as the structural recognition motif for endocytosis. Cell 63, 1061–1072.

Compagnon J, Gervais L, Roman MS, Chamot-Bœuf S, Guichet A (2009). Interplay between Rab5 and PtdIns(4,5)P_2 controls early endocytosis in the *Drosophila* germline. J Cell Sci 122, 25–35.

Coutelis JB, Ephrussi A (2007). Rab6 mediates membrane organization and determinant localization during *Drosophila* oogenesis. Development 134, 1419–1430.

Culi J, Mann RS (2003). Boca, an endoplasmic reticulum protein required for wingless signaling and trafficking of LDL receptor family members in *Drosophila*. Cell 112, 343–354.

Cuttell L, Vaughan A, Silva E, Escaron CJ, Lavine M, Van Goethem E, Eid JP, Quirin M, Franc NC (2008). Undertaker, a *Drosophila* Junctophilin, links Draper-mediated phagocytosis and calcium homeostasis. Cell 135, 524–534.

Dalal S, Rosser MF, Cyr DM, Hanson PI (2004). Distinct roles for the AAA ATPases NSF and p97 in the secretory pathway. Mol Biol Cell 15, 637–648.

DiMario PJ, Mahowald AP (1987). Female sterile (1) *yolkless*: a recessive female sterile mutation in *Drosophila melanogaster* with depressed numbers of coated pits and coated vesicles within the developing oocytes. J Cell Biol 105, 199–206.

Dollar G, Struckhoff E, Michaud J, Cohen RS (2002). Rab11 polarization of the *Drosophila* oocyte: a novel link between membrane trafficking, microtubule organization, and oskar mRNA localization and translation. Development 129, 517–526.

Drake MT, Downs MA, Traub LM (2000). Epsin binds to clathrin by associating directly with the clathrin-terminal domain: evidence for cooperative binding through two discrete sites. J Biol Chem 275, 6479–6489.

Drake MT, Traub LM (2001). Interaction of two structurally-distinct sequence types with the clathrin terminal domain β-propeller. J Biol Chem 276, 28700–28709.

Edeling MA, Mishra SK, Keyel PA, Steinhauser AL, Collins BM, Roth R, Heuser JE, Owen DJ, Traub LM (2006). Molecular switches involving the AP-2 β2 appendage regulate endocytic cargo selection and clathrin coat assembly. Dev Cell 10, 329–342.

Eden ER, Sun XM, Patel DD, Soutar AK (2007). Adaptor protein Disabled-2 modulates low density lipoprotein (LDL) receptor synthesis in fibroblasts from patients with autosomal recessive hypercholesterolemia. Hum Mol Genet 16, 2751–2759.

Ehrlich M, Boll W, Van Oijen A, Hariharan R, Chandran K, Nibert ML, Kirchhausen T (2004). Endocytosis by random initiation and stabilization of clathrin-coated pits. Cell 118, 591–605.

Elbashir SM, Harborth J, Lendeckel W, Yalcin A, Weber K, Tuschl T (2001). Duplexes of 21-nucleotide RNAs mediate RNA interference in cultured mammalian cells. Nature 411, 494–498.

Engqvist-Goldstein AE, Warren RA, Kessels MM, Keen JH, Heuser J, Drubin DG (2001). The actin-binding protein Hip1R associates with clathrin during early stages of endocytosis and promotes clathrin assembly in vitro. J Cell Biol 154, 1209–1224.

Ezratty EJ, Bertaux C, Marcantonio EE, Gundersen GG (2009). Clathrin mediates integrin endocytosis for focal adhesion disassembly in migrating cells. J Cell Biol 187, 733–747.

Farooq A, Zhou MM (2004). PTB or not to be: promiscuous, tolerant and bizarro domains come of age. IUBMB Life 56, 547–557.

Freeman MR, Delrow J, Kim J, Johnson E, Doe CQ (2003). Unwrapping glial biology: Gcm target genes regulating glial development, diversification, and function. Neuron 38, 567–580.

Fuentes-Medel Y, Logan MA, Ashley J, Ataman B, Budnik V, Freeman MR (2009). Glia and muscle sculpt neuromuscular arbors by engulfing destabilized synaptic boutons and shed presynaptic debris. PLoS Biol 7, e1000184.

Gaidarov I, Smith ME, Domin J, Keen JH (2001). The class II phosphoinositide 3-kinase C2alpha is activated by clathrin and regulates clathrin-mediated membrane trafficking. Mol Cell 7, 443–449.

Glittenberg M, Pitsouli C, Garvey C, Delidakis C, Bray S (2006). Role of conserved intracellular motifs in Serrate signalling, *cis*-inhibition and endocytosis. EMBO J 25, 4697–4706.

Gutzeit HO, Arendt D (1994). Blocked endocytotic uptake by the oocyte causes accumulation of vitellogenins in the haemolymph of the female-sterile mutants quitPX61 and stand stillPS34 of *Drosophila*. Cell Tissue Res 275, 291–298.

Hamon Y, Trompier D, Ma Z, Venegas V, Pophillat M, Mignotte V, Zhou Z, Chimini G (2006). Cooperation between engulfment receptors: the case of ABCA1 and MEGF10. PLoS One 1, e120.

Hansen B *et al*. (2005). Stabilin-1 and stabilin-2 are both directed into the early endocytic pathway in hepatic sinusoidal endothelium via interactions with clathrin/AP-2, independent of ligand binding. Exp Cell Res 303, 160–173.

Hao CY, Perkinton MS, Chan WW, Chan HY, Miller CC, Lau KF (2011). GULP1 is a novel APP interacting protein that alters APP processing. Biochem J 436, 631–639.

Hashimoto Y, Tabuchi Y, Sakurai K, Kutsuna M, Kurokawa K, Awasaki T, Sekimizu K, Nakanishi Y, Shiratsuchi A (2009). Identification of lipoteichoic acid as a ligand for draper in the phagocytosis of *Staphylococcus* aureus by *Drosophila* hemocytes. J Immunol 183, 7451–7460.

Hassan BA, Prokopenko SN, Breuer S, Zhang B, Paululat A, Bellen HJ (1998). *skittles*, a *Drosophila* phosphatidylinositol 4-phosphate 5-kinase, is required for cell viability, germline development and bristle morphology, but not for neurotransmitter release. Genetics 150, 1527–1537.

Hawryluk MJ, Keyel PA, Mishra SK, Watkins SC, Heuser JE, Traub LM (2006). Epsin 1 is a polyubiquitin-selective clathrin-associated sorting protein. Traffic 7, 262–281.

Hinrichsen L, Harborth J, Andrees L, Weber K, Ungewickell EJ (2003). Effect of clathrin heavy chain- and α-adaptin specific small interfering RNAs on endocytic accessory proteins and receptor trafficking in HeLa cells. J Biol Chem 278, 45160–45170.

Holmes A, Flett A, Coudreuse D, Korswagen HC, Pettitt J (2007). *C. elegans* Disabled is required for cell-type specific endocytosis and is essential in animals lacking the AP-3 adaptor complex. J Cell Sci 120, 2741–2751.

Huang F, Khvorova A, Marshall W, Sorkin A (2004). Analysis of clathrin-mediated endocytosis of epidermal growth factor receptor by RNA interference. J Biol Chem 279, 16657–16661.

Humphrey JS, Peters PJ, Yuan LC, Bonifacino JS (1993). Localization of TGN38 to the trans-Golgi network: Involvement of a cytoplasmic tyrosine-containing sequence. J Cell Biol 120, 1123–1135.

Ishihara H *et al*. (1989). Calyculin A and okadaic acid: inhibitors of protein phosphatase activity. Biochem Biophys Res Commun 159, 871–877.

Ishii K, Hamamoto H, Kamimura M, Nakamura Y, Noda H, Imamura K, Mita K, Sekimizu K (2010). Insect cytokine paralytic peptide (PP) induces cellular and humoral immune responses in the silkworm *Bombyx mori*. J Biol Chem 285, 28635–28642.

Jackson LP, Kelly BT, McCoy AJ, Gaffry T, James LC, Collins BM, Honing S, Evans PR, Owen DJ (2010). A large-scale conformational change couples membrane recruitment to cargo binding in the AP2 clathrin adaptor complex. Cell 141, 1220–1229.

Jha A, Agostinelli NR, Mishra SK, Keyel PA, Hawryluk MJ, Traub LM (2004). A novel AP-2 adaptor interaction motif initially identified in the long-splice isoform of synaptojanin 1, SJ170. J Biol Chem 279, 2281–2290.

Kaneko T, Sidhu SS, Li SS (2011). Evolving specificity from variability for protein interaction domains. Trends Biochem Sci 36, 183–190.

Kelly BT, McCoy AJ, Spate K, Miller SE, Evans PR, Honing S, Owen DJ (2008). A structural explanation for the binding of endocytic dileucine motifs by the AP2 complex. Nature 456, 976–979.

Kessell I, Holst BD, Roth TF (1989). Membranous intermediates in endocytosis are labile, as shown in a temperature-sensitive mutant. Proc Natl Acad Sci USA 86, 4968–4972.

Keyel PA, Mishra SK, Roth R, Heuser JE, Watkins SC, Traub LM (2006). A single common portal for clathrin-mediated endocytosis of distinct cargo governed by cargo-selective adaptors. Mol Biol Cell 17, 4300–4317.

Keyel PA, Thieman JR, Roth R, Erkan E, Everett ET, Watkins SC, Traub LM (2008). The AP-2 adaptor β2 appendage scaffolds alternate cargo endocytosis. Mol Biol Cell 19, 5309–5326.

Kinchen JM (2010). A model to die for: signaling to apoptotic cell removal in worm, fly and mouse. Apoptosis 15, 998–1006.

Kinchen JM, Cabello J, Klingele D, Wong K, Feichtinger R, Schnabel H, Schnabel R, Hengartner MO (2005). Two pathways converge at CED-10 to mediate actin rearrangement and corpse removal in *C. elegans*. Nature 434, 93–99.

King RC (1970). Ovarian Development in *Drosophila melanogaster*, New York: Academic Press.

Kiss RS, Ma Z, Nakada-Tsukui K, Brugnera E, Vassiliou G, McBride HM, Ravichandran KS, Marcel YL (2006). The lipoprotein receptor-related protein-1 (LRP) adapter protein GULP mediates trafficking of the LRP ligand prosaposin, leading to sphingolipid and free cholesterol accumulation in late endosomes and impaired efflux. J Biol Chem 281, 12081–12092.

Kozik P, Francis RW, Seaman MN, Robinson MS (2010). A screen for endocytic motifs. Traffic 11, 843–855.

Kuraishi T *et al*. (2009). Pretaporter, a *Drosophila* protein serving as a ligand for Draper in the phagocytosis of apoptotic cells. EMBO J 28, 3868–3878.

Lauritsen JP, Menne C, Kastrup J, Dietrich J, Odum N, Geisler C (2000). β2-Adaptin is constitutively de-phosphorylated by serine/threonine protein

phosphatase PP2A and phosphorylated by a staurosporine-sensitive kinase. Biochim Biophys Acta 1497, 297–307.
Lee S, Cooley L (2007). Jagunal is required for reorganizing the endoplasmic reticulum during *Drosophila* oogenesis. J Cell Biol 176, 941–952.
Li H *et al*. (2008). Structure of the C-terminal phosphotyrosine interaction domain of Fe65L1 complexed with the cytoplasmic tail of amyloid precursor protein reveals a novel peptide binding mode. J Biol Chem 283, 27165–27178.
Li Y, Lu W, Marzolo MP, Bu G (2001). Differential functions of members of the low density lipoprotein receptor family suggested by their distinct endocytosis rates. J Biol Chem 276, 18000–18006.
Lindwasser OW, Smith WJ, Chaudhuri R, Yang P, Hurley JH, Bonifacino JS (2008). A diacidic motif in human immunodeficiency virus type 1 Nef is a novel determinant of binding to AP-2. J Virol 82, 1166–1174.
Liu QA, Hengartner MO (1998). Candidate adaptor protein CED-6 promotes the engulfment of apoptotic cells in *C. elegans*. Cell 93, 961–972.
Liu QA, Hengartner MO (1999). Human CED-6 encodes a functional homologue of the *Caenorhabditis elegans* engulfment protein CED-6. Curr Biol 9, 1347–1350.
Loerke D, Mettlen M, Yarar D, Jaqaman K, Jaqaman H, Danuser G, Schmid SL (2009). Cargo and dynamin regulate clathrin-coated pit maturation. PLoS Biol 7, e57.
Lu N, Shen Q, Mahoney TR, Liu X, Zhou Z (2011). Three sorting nexins drive the degradation of apoptotic cells in response to PtdIns(3)P signaling. Mol Biol Cell 22, 354–374.
Lu N, Shen Q, Mahoney TR, Neukomm LJ, Wang Y, Zhou Z (2012). Two PI 3-kinases and one PI 3-phosphatase together establish the cyclic waves of phagosomal PtdIns(3)P critical for the degradation of apoptotic cells. PLoS Biol 10, e1001245.
Lu N, Zhou Z (2012). Membrane trafficking and phagosome maturation during the clearance of apoptotic cells. Int Rev Cell Mol Biol 293, 269–309.
Lundmark R, Carlsson SR (2002). The β-appendages of the four adaptor-protein (AP) complexes: structure and binding properties, and identification of sorting nexin 9 as an accessory protein to AP-2. Biochem J 362, 597–607.
Lundmark R, Carlsson SR (2003). Sorting nexin 9 participates in clathrin-mediated endocytosis through interactions with the core components. J Biol Chem 278, 46772–46781.
Ma Z, Nie Z, Luo R, Casanova JE, Ravichandran KS (2007). Regulation of Arf6 and ACAP1 signaling by the PTB-domain-containing adaptor protein GULP. Curr Biol 17, 722–727.
MacDonald JM, Beach MG, Porpiglia E, Sheehan AE, Watts RJ, Freeman MR (2006). The *Drosophila* cell corpse engulfment receptor Draper mediates glial clearance of severed axons. Neuron 50, 869–881.
Mahowald AP (1972). Ultrastructural observations on oogenesis in *Drosophila*. J Morphol 137, 29–48.
Manaka J, Kuraishi T, Shiratsuchi A, Nakai Y, Higashida H, Henson P, Nakanishi Y (2004). Draper-mediated and phosphatidylserine-independent phagocytosis of apoptotic cells by *Drosophila* hemocytes/macrophages. J Biol Chem 279, 48466–48476.
Marks MS, Woodruff L, Ohno H, Bonifacino JS (1996). Protein targeting by tyrosine- and di-leucine-based signals: evidence for distinct saturable components. J Cell Biol 135, 341–354.
Martins-Silva C *et al*. (2006). A rat homologue of CED-6 is expressed in neurons and interacts with clathrin. Brain Res 1119, 1–12.
Maurer ME, Cooper JA (2006). The adaptor protein Dab2 sorts LDL receptors into coated pits independently of AP-2 and ARH. J Cell Sci 119, 4235–4246.
Miele AE, Watson PJ, Evans PR, Traub LM, Owen DJ (2004). Two distinct interaction motifs in amphiphysin bind two independent sites on the clathrin terminal domain β-propeller. Nat Struct Mol Biol 11, 242–248.
Mishra NK (2011). Similarities between oocytes and macrophages. An overview. Folia Histochem Cytobiol 49, 8–9.
Mishra SK, Agostinelli NR, Brett TJ, Mizukami I, Ross TS, Traub LM (2001). Clathrin- and AP-2-binding sites in HIP1 uncover a general assembly role for endocytic accessory proteins. J Biol Chem 276, 46230–46236.
Mishra SK, Jha A, Steinhauser AL, Kokoza VA, Washabaugh CH, Raikhel AS, Foster WA, Traub LM (2008). Internalization of LDL-receptor superfamily yolk-protein receptors during mosquito oogenesis involves transcriptional regulation of PTB-domain adaptors. J Cell Sci 121, 1264–1274.
Mishra SK, Keyel PA, Edeling MA, Owen DJ, Traub LM (2005). Functional dissection of an AP-2 β2 appendage-binding sequence within the autosomal recessive hypercholesterolemia (ARH) protein. J Biol Chem 280, 19270–19280.
Mishra SK, Keyel PA, Hawryluk MJ, Agostinelli NR, Watkins SC, Traub LM (2002a). Disabled-2 exhibits the properties of a cargo-selective endocytic clathrin adaptor. EMBO J 21, 4915–4926.
Mishra SK, Watkins SC, Traub LM (2002b). The autosomal recessive hypercholesterolemia (ARH) protein interfaces directly with the clathrin-coat machinery. Proc Natl Acad Sci USA 99, 16099–16104.
Motley A, Bright NA, Seaman MN, Robinson MS (2003). Clathrin-mediated endocytosis in AP-2-depleted cells. J Cell Biol 162, 909–918.
Nathke IS, Heuser J, Lupas A, Stock J, Turck CW, Brodsky FM (1992). Folding and trimerization of clathrin subunits at the triskelion hub. Cell 68, 899–910.
Nezis IP, Shravage BV, Sagona AP, Lamark T, Bjorkoy G, Johansen T, Rusten TE, Brech A, Baehrecke EH, Stenmark H (2010). Autophagic degradation of dBruce controls DNA fragmentation in nurse cells during late *Drosophila melanogaster* oogenesis. J Cell Biol 190, 523–531.
Nezis IP, Stravopodis DJ, Papassideri I, Robert-Nicoud M, Margaritis LH (2000). Stage-specific apoptotic patterns during *Drosophila* oogenesis. Eur J Cell Biol 79, 610–620.
Nezis IP, Stravopodis DJ, Papassideri I, Robert-Nicoud M, Margaritis LH (2002). Dynamics of apoptosis in the ovarian follicle cells during the late stages of *Drosophila* oogenesis. Cell Tissue Res 307, 401–409.
Ohno H, Stewart J, Fournier M-C, Bosshart H, Rhee I, Miyatake S, Saito T, Galluser A, Kirchhausen T, Bonifacino JS (1995). Interaction of tyrosine-based sorting signals with clathrin-associated proteins. Science 269, 1872–1875.
Park SY, Kang KB, Thapa N, Kim SY, Lee SJ, Kim IS (2008). Requirement of adaptor protein GULP during stabilin-2-mediated cell corpse engulfment. J Biol Chem 283, 10593–10600.
Park SY, Kim SY, Kang KB, Kim IS (2010). Adaptor protein GULP is involved in stabilin-1-mediated phagocytosis. Biochem Biophys Res Commun 398, 467–472.
Parra-Peralbo E, Culi J (2011). *Drosophila* lipophorin receptors mediate the uptake of neutral lipids in oocytes and imaginal disc cells by an endocytosis-independent mechanism. PLoS Genet 7, e1001297.
Pechstein A *et al*. (2010). Regulation of synaptic vesicle recycling by complex formation between intersectin 1 and the clathrin adaptor complex AP2. Proc Natl Acad Sci USA 107, 4206–4211.
Pedersen GA, Chakraborty S, Steinhauser AL, Traub LM, Madsen M (2010). AMN directs endocytosis of the intrinsic factor-vitamin B receptor cubam by engaging ARH or Dab2. Traffic 11, 706–720.
Perry MM, Gilbert AB (1979). Yolk transport in the ovarian follicle of the hen (*Gallus domesticus*): lipoprotein-like particles at the periphery of the oocyte in the rapid growth phase. J Cell Sci 39, 257–272.
Pizarro-Cerda J, Bonazzi M, Cossart P (2010). Clathrin-mediated endocytosis: what works for small, also works for big. Bioessays 32, 496–504.
Raikhel AS, Dhadialla TS (1992). Accumulation of yolk proteins in insect oocytes. Annu Rev Entomol 37, 217–251.
Rasheed S, Nelson-Rees WA, Toth EM, Arnstein P, Gardner MB (1974). Characterization of a newly derived human sarcoma cell line (HT-1080). Cancer 33, 1027–1033.
Reider A, Wendland B (2011). Endocytic adaptors—social networking at the plasma membrane. J Cell Sci 124, 1613–1622.
Richard DS, Gilbert M, Crum B, Hollinshead DM, Schelble S, Scheswohl D (2001). Yolk protein endocytosis by oocytes in *Drosophila* melanogaster: immunofluorescent localization of clathrin, adaptin and the yolk protein receptor. J Insect Physiol 47, 715–723.
Rocha JJ, Korolchuk VI, Robinson IM, O'Kane CJ (2011). A phagocytic route for uptake of double-stranded RNA in RNAi. PLoS One 6, e19087.
Rorth P (1998). Gal4 in the *Drosophila* female germline. Mech Dev 78, 113–118.
Roth TF, Porter KR (1964). Yolk protein uptake in the oocyte of the mosquito *Aedes aegypti* L. J Cell Biol 20, 313–332.
Ruan J *et al*. (2008). TreeFam: 2008 update. Nucleic Acids Res 36, D735–D740.
Sappington TW, Kokoza VA, Cho WL, Raikhel AS (1996). Molecular characterization of the mosquito vitellogenin receptor reveals unexpected high homology to the *Drosophila* yolk protein receptor. Proc Natl Acad Sci USA 93, 8934–8939.
Saunders DS, Henrich VC, Gilbert LI (1989). Induction of diapause in *Drosophila melanogaster*: photoperiodic regulation and the impact of arrhythmic clock mutations on time measurement. Proc Natl Acad Sci USA 86, 3748–3752.
Schmid EM, Ford MG, Burtey A, Praefcke GJ, Peak Chew SY, Mills IG, Benmerah A, McMahon HT (2006). Role of the AP2 β-appendage hub in recruiting partners for clathrin coated vesicle assembly. PLoS Biol. 4, e262.

Schmid EM, McMahon HT (2007). Integrating molecular and network biology to decode endocytosis. Nature 448, 883–888.
Schonbaum CP, Lee S, Mahowald AP (1995). The *Drosophila* yolkless gene encodes a vitellogenin receptor belonging to the low density lipoprotein receptor superfamily. Proc Natl Acad Sci USA 92, 1485–1489.
Schonbaum CP, Perrino JJ, Mahowald AP (2000). Regulation of the vitellogenin receptor during *Drosophila melanogaster* oogenesis. Mol Biol Cell 11, 511–521.
Seo SJ, Cheon HM, Sun J, Sappington TW, Raikhel AS (2003). Tissue- and stage-specific expression of two lipophorin receptor variants with seven and eight ligand-binding repeats in the adult mosquito. J Biol Chem 278, 41954–41962.
Shaner NC, Campbell RE, Steinbach PA, Giepmans BN, Palmer AE, Tsien RY (2004). Improved monomeric red, orange and yellow fluorescent proteins derived from *Discosoma* sp. red fluorescent protein. Nat Biotechnol 22, 1567–1572.
Slepnev VI, Ochoa GC, Butler MH, Grabs D, Camilli PD (1998). Role of phosphorylation in regulation of the assembly of endocytic coat complexes. Science 281, 821–824.
Smits E, Van Criekinge W, Plaetinck G, Bogaert T (1999). The human homologue of *Caenorhabditis elegans* CED-6 specifically promotes phagocytosis of apoptotic cells. Curr Biol 9, 1351–1354.
Snigirevskaya ES, Sappington TW, Raikhel AS (1997). Internalization and recycling of vitellogenin receptor in the mosquito oocyte. Cell Tissue Res 290, 175–183.
Sommer B, Oprins A, Rabouille C, Munro S (2005). The exocyst component Sec5 is present on endocytic vesicles in the oocyte of *Drosophila melanogaster*. J Cell Biol 169, 953–963.
Stolt PC, Vardar D, Blacklow SC (2004). The dual-function disabled-1 PTB domain exhibits site independence in binding phosphoinositide and peptide ligands. Biochemistry 43, 10979–10987.
Su HP, Brugnera E, Van Criekinge W, Smits E, Hengartner M, Bogaert T, Ravichandran KS (2000). Identification and characterization of a dimerization domain in CED-6, an adapter protein involved in engulfment of apoptotic cells. J Biol Chem 275, 9542–9549.
Su HP, Nakada-Tsukui K, Tosello-Trampont AC, Li Y, Bu G, Henson PM, Ravichandran KS (2002). Interaction of CED-6/GULP, an adapter protein involved in engulfment of apoptotic cells, with CED-1 and CD91/low density lipoprotein receptor-related protein (LRP). J Biol Chem 277, 11772–11779.
Suzuki E, Nakayama M (2007). MEGF10 is a mammalian ortholog of CED-1 that interacts with clathrin assembly protein complex 2 medium chain and induces large vacuole formation. Exp Cell Res 313, 3729–3742.
Tamborindeguy C, Monsion B, Brault V, Hunnicutt L, Ju HJ, Nakabachi A, Van Fleet E (2010). A genomic analysis of transcytosis in the pea aphid, *Acyrthosiphon pisum*, a mechanism involved in virus transmission. Insect Mol Biol 19, (Suppl 2)259–272.
Tedesco JL, Courtright JB, Kumran AK (1981). Ultrastructural changes induced by juvenile hormone analogue in oocyte membranes of *apterous*^{4} *Drosophila melanogaster*. J Insect Physiol 27, 895–902.
Thieman JR, Mishra SK, Ling K, Doray B, Anderson RA, Traub LM (2009). Clathrin regulates the association of PIPKIγ661 with the AP-2 adaptor β2 appendage. J Biol Chem 284, 13924–13939.
Thinakaran G, Koo EH (2008). Amyloid precursor protein trafficking, processing, and function. J Biol Chem 283, 29615–29619.
Traub LM (2009). Tickets to ride: selecting cargo for clathrin-regulated internalization. Nat Rev Mol Cell Biol 10, 583–596.
Traub LM, Downs MA, Westrich JL, Fremont DH (1999). Crystal structure of the α appendage of AP-2 reveals a recruitment platform for clathrin-coat assembly. Proc Natl Acad Sci USA 96, 8907–8912.
Traub LM, Kornfeld S, Ungewickell E (1995). Different domains of the AP-1 adaptor complex are required for Golgi membrane binding and clathrin recruitment. J Biol Chem 270, 4933–4942.
Tsuruhara T, Koenig JH, Ikeda K (1990). Synchronized endocytosis studied in the oocyte of a temperature-sensitive mutant of *Drosophila melanogaster*. Cell Tissue Res 259, 199–207.
Tufail M, Takeda M (2009). Insect vitellogenin/lipophorin receptors: molecular structures, role in oogenesis, and regulatory mechanisms. J Insect Physiol 55, 87–103.
Uchiyama T, Broder S, Waldmann TA (1981). A monoclonal antibody (anti-Tac) reactive with activated and functionally mature human T cells. I. Production of anti-Tac monoclonal antibody and distribution of Tac (+) cells. J Immunol 126, 1393–1397.
Uhlen M *et al*. (2010). Towards a knowledge-based Human Protein Atlas. Nat Biotechnol 28, 1248–1250.
van der Bliek AM, Meyerowitz EM (1991). Dynamin-like protein encoded by the *Drosophila* shibire gene associated with vesicular traffic. Nature 351, 411–444.
Vandre DD, Ackerman WEt, Tewari A, Kniss DA, Robinson JM (2012). A placental sub-proteome: the apical plasma membrane of the syncytiotrophoblast. Placenta 33, 207–213.
Vanzo N, Oprins A, Xanthakis D, Ephrussi A, Rabouille C (2007). Stimulation of endocytosis and actin dynamics by oskar polarizes the *Drosophila* oocyte. Dev Cell 12, 543–555.
Waring GL, DiOrio JP, Hennen S (1983). Isolation of germ line-dependent female-sterile mutation that affects yolk specific sequestration and chorion formation in *Drosophila*. Dev Biol 100, 452–463.
Warren RA, Green FA, Stenberg PE, Enns CA (1998). Distinct saturable pathways for the endocytosis of different tyrosine motifs. J Biol Chem 273, 17056–17063.
Wessel D, Flugge UI (1984). A method for the quantitative recovery of protein in dilute solution in the presence of detergents and lipids. Anal Biochem 138, 141–143.
Wilbur JD, Chen CY, Manalo V, Hwang PK, Fletterick RJ, Brodsky FM (2008). Actin binding by huntingtin-interacting protein 1 (Hip1) and Hip1-related protein (Hip1R) is regulated by clathrin light chain. J Biol Chem 283, 32870–32879.
Windler SL, Bilder D (2010). Endocytic internalization routes required for delta/notch signaling. Curr Biol 20, 538–543.
Yu X, Lu N, Zhou Z (2008). Phagocytic receptor CED-1 initiates a signaling pathway for degrading engulfed apoptotic cells. PLoS Biol 6, e61.
Yu X, Odera S, Chuang CH, Lu N, Zhou Z (2006). *C. elegans* dynamin mediates the signaling of phagocytic receptor CED-1 for the engulfment and degradation of apoptotic cells. Dev Cell 10, 743–757.
Zhai B, Villen J, Beausoleil SA, Mintseris J, Gygi SP (2008). Phosphoproteome analysis of *Drosophila melanogaster* embryos. J Proteome Res 7, 1675–1682.
Zhao B, Wong AY, Murshid A, Bowie D, Presley JF, Bedford FK (2008). Identification of a novel di-leucine motif mediating K^{+}/Cl– cotransporter KCC2 constitutive endocytosis. Cell Signal 20, 1769–1779.
Zhou Y, Zhang J, King ML (2003). *Xenopus* autosomal recessive hypercholesterolemia protein couples lipoprotein receptors with the AP-2 complex in oocytes and embryos and is required for vitellogenesis. J Biol Chem 278, 44584–44592.
Zhou Z, Yu X (2008). Phagosome maturation during the removal of apoptotic cells: receptors lead the way. Trends Cell Biol 18, 474–485.
Ziegenfuss JS, Biswas R, Avery MA, Hong K, Sheehan AE, Yeung YG, Stanley ER, Freeman MR (2008). Draper-dependent glial phagocytic activity is mediated by Src and Syk family kinase signalling. Nature 453, 935–939.